

---

# Sample, estimate, aggregate: A recipe for causal discovery foundation models

---

Menghua Wu<sup>†,\*</sup>, Yujia Bao<sup>\*</sup>, Regina Barzilay<sup>†</sup>, Tommi Jaakkola<sup>†</sup>

<sup>†</sup>Massachusetts Institute of Technology  
Cambridge, MA 02139

<sup>\*</sup>Accenture  
Mountain View, CA 94041

## Abstract

Causal discovery, the task of inferring causal structure from data, promises to accelerate scientific research, inform policy making, and more. However, causal discovery algorithms over larger sets of variables tend to be brittle against misspecification or when data are limited. To mitigate these challenges, we train a supervised model that learns to predict a larger causal graph from the outputs of classical causal discovery algorithms run over subsets of variables, along with other statistical hints like inverse covariance. Our approach is enabled by the observation that typical errors in the outputs of classical methods remain comparable across datasets. Theoretically, we show that this model is well-specified, in the sense that it can recover a causal graph consistent with graphs over subsets. Empirically, we train the model to be robust to erroneous estimates using diverse synthetic data. Experiments on real and synthetic data demonstrate that this model maintains high accuracy in the face of misspecification or distribution shift, and can be adapted at low cost to different discovery algorithms or choice of statistics.<sup>2</sup>

## 1 Introduction

A fundamental aspect of scientific research is to discover and validate causal hypotheses involving variables of interest. Given observations of these variables, the goal of causal discovery algorithms is to extract such hypotheses in the form of directed graphs, in which edges denote causal relationships (Spirtes et al., 2001). There are several challenges to their widespread adoption in basic science. The core issue is that the correctness of these algorithms is tied to their assumptions on the data-generating processes, which are unknown in real applications. In principle, one could circumvent this issue by exhaustively running discovery algorithms with different assumptions and comparing their outputs with surrogate measures that reflect graph quality (Faller et al., 2023). However, this search would be costly: current algorithms must be optimized from scratch each time, and they scale poorly to the graph and sample sizes present in modern scientific big data (Replogle et al., 2022).

Causal discovery algorithms follow two primary approaches that differ in their treatment of the causal graph. Discrete optimization algorithms explore the super-exponential space of graphs by proposing and evaluating changes to a working graph (Glymour et al., 2019). While these methods are fast on small graphs, the combinatorial space renders them intractable for exploring larger structures. Furthermore, these algorithms are driven by hypothesis tests, which necessarily impose functional assumptions on the data-generating process, and whose results can be erroneous, especially as the number of variables increases. An alternative is to frame causal discovery as a continuous optimization over weighted adjacency matrices. These algorithms either fit a generative model to the

---

\*Correspondence to [rmwu@mit.edu](mailto:rmwu@mit.edu)

<sup>2</sup>Our code is available at <https://github.com/rmwu/sea>.

data and extract the causal graph as a parameter (Zheng et al., 2018), or train a supervised learning model on simulated data (Lorch et al., 2022). However, the former must be trained from scratch per-dataset, and latter are not easily extensible to causal mechanisms beyond those in the training set.

In this work, we present SEA: Sample, Estimate, Aggregate, a supervised causal discovery framework that aims to perform well even when data-generating processes are unknown, and to easily incorporate prior knowledge when it is available. We train a deep learning model to predict causal graphs from two types of statistical descriptors: the estimates of classical discovery algorithms over small subsets, and graph-level statistics. Classical discovery algorithms output a representation of a graph’s equivalency class, whose format is largely consistent across algorithms, and whose errors are comparable across datasets. Statistics like correlation or inverse covariance are strong indicators for a graph’s overall connectivity and can reduce the number of subsets on which we must run discovery algorithms. Theoretically, we show that our model can implement a combinatorial algorithm that recovers larger causal graphs that are consistent with smaller, marginal subgraphs. Empirically, our training procedure forces the model to predict causal graphs across diverse synthetic data, including on datasets that are misaligned with the discovery algorithms’ assumptions, or when insufficient subsets are provided.

We implement instantiations of SEA using an efficient, axial-attention based model (Ho et al., 2020), with inverse covariance and estimates from the FCI or GIES algorithms (Spirtes et al., 1995; Hauser & Bühlmann, 2012). We first conduct thorough comparison to three classical baselines and five deep learning approaches on in-distribution and out-of-distribution data. SEA attains the state-of-the-art results on synthetic and real causal discovery tasks, while providing 10-1000x faster inference. Then we show that it is possible to replace the classical discovery algorithm without any modification to the trained model, for performance gain on datasets that match the assumptions of the new algorithm. We also show that this model can be finetuned at a fraction of the training cost to accommodate new graph-level statistics that capture different (e.g. nonlinear) relationships. Thus, while these experiments focus on specific algorithms and architectures, the overall framework accepts any combination of sampling heuristics, classical causal discovery algorithms, and statistical features.

## 2 Background and related work

### 2.1 Causal graphical models

A causal graphical model is a directed, acyclic graph  $G = (V, E)$ , where each node  $i \in V$  corresponds to a random variable  $X_i \in X$  and each edge  $(i, j) \in E$  represents a causal relationship from  $X_i \rightarrow X_j$ . We assume that the data distribution  $P_X$  is Markov to  $G$ ,

$$\forall i \in V, X_i \perp\!\!\!\perp V \setminus (X_{\delta_i} \cup X_{\pi_i}) \mid X_{\pi_j} \tag{1}$$

where  $\delta_i$  is the set of descendants of node  $i$  in  $G$ , and  $\pi_i$  is the set of parents of  $i$ . In addition, we assume that  $P_X$  is minimal and faithful – that is,  $P_X$  does not include any independence relationships beyond those implied by applying the Markov condition to  $G$  (Spirtes et al., 2001). Causal graphical models allow us to perform *interventions* on nodes  $i$  by setting conditional  $P(X_i \mid X_{\pi_i})$  to a different distribution  $\tilde{P}(X_i \mid X_{\pi_i})$ . In this paper, our experiments cover the observational case (no interventions) and the case with perfect interventions on each node, i.e.  $\tilde{P}(X_i \mid X_{\pi_i}) = \tilde{P}(X_i)$ .

### 2.2 Causal structure learning

Given a dataset  $D \sim P_X$ , our goal is to recover  $G$ . There are two main challenges. First, the number of possible graphs is super-exponential in the number of nodes  $N$ , so causal discovery algorithms must navigate this combinatorial search space efficiently. Second, depending on data availability and the underlying data generation process, causal discovery algorithms may or may not be able to recover  $G$  in practice. In fact, many algorithms are only analyzed in the infinite-data regime and require at least thousands of data samples for reasonable empirical performance (Spirtes et al., 2001; Brouillard et al., 2020). Causal discovery is also used in the context of pairwise relationships (Zhang & Hyvarinen, 2012; Monti et al., 2019), as well as for non-stationary (Huang et al., 2020b) and time-series (Löwe et al., 2022) data. This work focuses on causal discovery for stationary graphs, so we will discuss the two main approaches in this setting.

**Discrete optimization methods** make atomic changes to a proposal graph until a stopping criterion is met. Constraint-based algorithms identify edges based on conditional independence tests, and

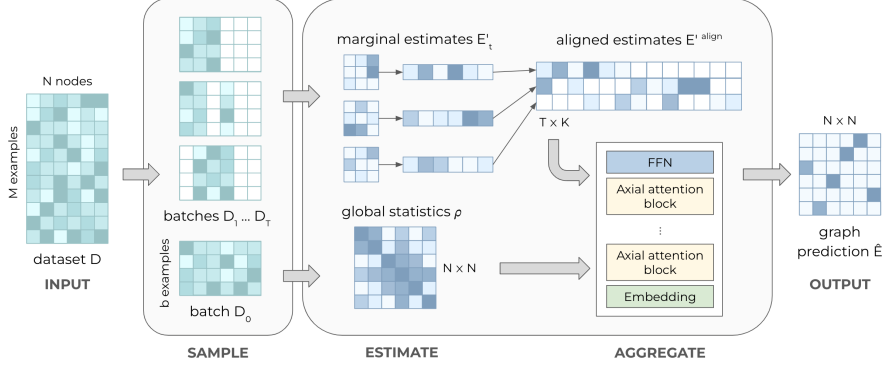


Figure 1: The inference procedure. Given a new dataset, we 1) sample batches and subsets of nodes, 2) estimate marginal graphs and global statistics over these batches, and 3) a pretrained aggregator predicts the causal graph from these estimates. Raw data in green; graph-related features in blue.

their correctness is inseparable from the empirical results of those tests (Glymour et al., 2019), whose statistical power depends directly on dataset size. These include the FCI and PC algorithms in the observational case (Spirtes et al., 1995), and the JCI in the interventional case (Mooij et al., 2020). Score-based methods also make iterative modifications to a working graph, but their goal is to maximize a continuous score over the discrete space of all valid graphs, with the true graph at the optimum. Due to the intractable search space, these methods often make decisions based on greedy heuristics. Classic examples include GES (Chickering, 2002), GIES (Hauser & Bühlmann, 2012), CAM (Bühlmann et al., 2014), LiNGAM (Shimizu et al., 2006), and IGSP (Wang et al., 2017).

**Continuous optimization approaches** recast the combinatorial space of graphs into a continuous space of weighted adjacency matrices. Many of these works train a generative model to learn the empirical data distribution, which is parameterized through the adjacency matrix (Zheng et al., 2018; Lachapelle et al., 2020; Brouillard et al., 2020). Others focus on properties related to the empirical data distribution, such as a relationship between the underlying graph and the Jacobian of the learned model (Reizinger et al., 2023), or between the Hessian of the data log-likelihood and the topological order (Sanchez et al., 2023). Finally, most similar to this work, amortized inference approaches (Ke et al., 2022; Lorch et al., 2022) frame causal discovery as a supervised learning problem within a class of data-generating mechanisms. However, they must be re-trained to incorporate new information, and since they operate on raw observations, they scale poorly to larger datasets.

### 2.3 Foundation models

The concept of foundation models has revolutionized the machine learning workflow in a variety of disciplines: instead of training domain-specific models from scratch, we can query a pretrained, general-purpose “foundation” model (Radford et al., 2021; Brown et al., 2020; Bommasani et al., 2022). In this work, our goal is to describe a prototype of a causal discovery foundation model, which operates across a variety of situations and can be adapted towards specific downstream tasks.

## 3 Methods

### 3.1 Inference procedure

SEA is a causal discovery framework that learns to resolve statistical features and estimates of marginal graphs into a global causal graph. The inference procedure is depicted in Figure 1. Specifically, given a new dataset  $D \in \mathbb{R}^{M \times N}$  faithful to graph  $G = (V, E)$ , we apply the following stages.

**Sample:** takes as input dataset  $D$ ; and outputs data batches  $\{D_0, D_1, \dots, D_T\}$  and node subsets  $\{S_1, \dots, S_T\}$ .

1. Sample  $T + 1$  batches of  $b \ll M$  observations uniformly at random from  $D$ .
2. Compute selection scores  $\alpha \in (0, 1)^{N \times N}$  over  $D_0$  (e.g. correlation or inverse covariance).
3. Sample  $T$  node subsets of size  $k$ . Each subset  $S_t \subseteq V$  is constructed iteratively, where nodes are added with probability proportional to  $\sum_{j \in S_t} \alpha_{i,j}$  (details and alternatives in B.6).

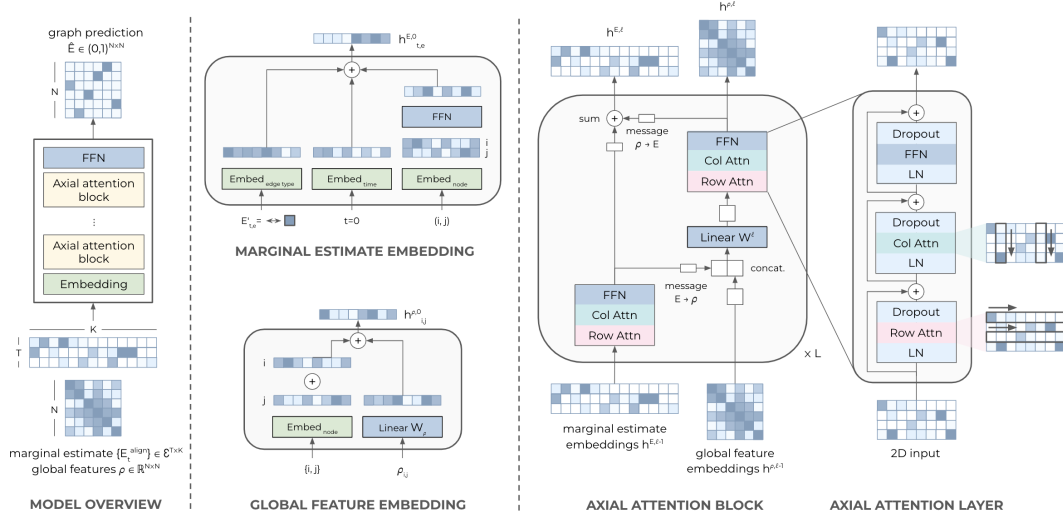


Figure 2: Aggregator architecture. Marginal graph estimates and global statistics are embedded into the model dimension. 1D positional embeddings are added along both rows and columns. Embedded features pass through a series of axial attention blocks, which attend to the marginal and global features. Final layer global features pass through a feedforward network to predict the causal graph.

**Estimate:** takes as inputs data batches, node subsets, and (optionally) intervention targets; and outputs global statistics  $\rho$  and marginal estimates  $\{E'_1, \dots, E'_T\}$ .

1. Compute global statistics  $\rho \in \mathbb{R}^{N \times N}$  over  $D_0$  (e.g. correlation or inverse covariance).
2. Run discovery algorithm  $f$  to obtain marginal estimates  $f(D_t[S_t]) = E'_t$  for  $t = 1 \dots T$ .

We use  $D_t[S_t]$  to denote the observations in  $D_t$  that correspond only to the variables in  $S_t$ . Each estimate  $E'_t$  is a  $k \times k$  adjacency matrix, corresponding to the  $k$  nodes in  $S_t$ .

**Aggregate:** takes as inputs global statistics, marginal estimates, and node subsets. A pretrained aggregator model outputs the predicted global causal graph  $\hat{E} \in (0, 1)^{N \times N}$  (Section 3.3).

### 3.2 Training procedure

The training procedure mirrors the inference procedure. Each input is a whole dataset (summarized into global statistics and a set of marginal estimates), and the supervised output is the ground truth graph. Sampling and estimation are run in parallel on CPU, while aggregation is run on GPU.

We trained two aggregator models, which employed the FCI algorithm with the Fisherz test and GIES algorithm with the Bayesian information criterion (Schwarz, 1978). Both estimation algorithms were chosen for speed and assume that the data are linear and Gaussian. Note that the algorithm used for inference can differ from the one used during training, as long as their outputs are the same format, e.g. a CPDAG (Andersson et al., 1997) (experiments in Section 5.2). The training dataset contains both data that are correctly and incorrectly specified (details in Section 4.1), so the aggregator is forced to predict the correct graph regardless. In addition, each training instance is provided a random number of marginal estimates, which might not cover every edge. As a result, the aggregator must extrapolate to unseen edges using the available estimates and the global statistics. For example, if two variables have low correlation, and they are located in different neighborhoods of the already-identified graph, it may be reasonable to assume that they are unconnected.

### 3.3 Model architecture

The aggregator is a neural network that takes as input: global statistics  $\rho \in \mathbb{R}^{N \times N}$ , marginal estimates  $E'_{1..T} \in \mathcal{E}^{T \times k \times k}$ , and node subsets  $S_{1..T} \in [N]^{T \times k}$  (Figure 2), where  $\mathcal{E}$  is the set of output edge types for the causal discovery algorithm  $f$ .<sup>3</sup>

<sup>3</sup>E.g. “no relationship,” “ $X$  causes  $Y$ ,” “ $X$  is not a descendent of  $Y$ ”

We project global statistics into the model dimension via a learned linear projection matrix  $W_\rho : \mathbb{R} \rightarrow \mathbb{R}^d$ , and we embed edge types via a learned embedding  $\text{ebd}_\mathcal{E} : \mathcal{E} \rightarrow \mathbb{R}^d$ . To collect estimates of the same edge over all subsets, we align entries of  $E'_{1\dots T}$  into  $E_T^{\text{align}} \in \mathcal{E}^{T \times K}$

$$E'_{t,e=(i,j)} = \begin{cases} E'_{t,i,j} & \text{if } i \in S_t, j \in S_t \\ 0 & \text{otherwise} \end{cases} \quad (2)$$

where  $t$  indexes into the subsets,  $e$  indexes into the set of unique edges, and  $K$  is the number of unique edges. We add learned 1D positional embeddings along both dimensions of each input,

$$\begin{aligned} \text{pos-ebd}(\rho_{i,j}) &= \text{ebd}_{\text{node}}(i') + \text{ebd}_{\text{node}}(j') \\ \text{pos-ebd}(E_{t,e}^{\text{align}}) &= \text{ebd}_{\text{time}}(t) + \text{FFN}([\text{ebd}_{\text{node}}(i'), \text{ebd}_{\text{node}}(j')]) \end{aligned}$$

where  $i', j'$  index into a random permutation on  $V$  for invariance to node permutation and graph size.<sup>4</sup> Due to the (a)symmetries of their inputs,  $\text{pos-ebd}(\rho_{i,j})$  is symmetric, while  $\text{pos-ebd}(E_{t,e}^{\text{align}})$  considers the node ordering. In summary, the inputs to our axial attention blocks are

$$h_{i,j}^\rho = (W_\rho \rho)_{i,j} + \text{pos-ebd}(\rho_{i,j}) \quad (3)$$

$$h_{t,e}^E = \text{ebd}_\mathcal{E}(E_{t,e}^{\text{align}}) + \text{pos-ebd}(E_{t,e}^{\text{align}}) \quad (4)$$

for  $i, j \in [N]^2, t \in [T], e \in [K]$ .

**Axial attention** An axial attention block contains two axial attention layers (marginal estimates, global statistics) and a feed-forward network (Figure 2, right). Given a 2D input, an axial attention layer attends first along the rows, then along the columns. For example, on a matrix of size  $(R, C, d)$ , one pass of the axial attention layer is equivalent to running standard self-attention along  $C$  with batch size  $R$ , followed by the reverse. For marginal estimates,  $R$  is the number of subsets  $T$ , and  $C$  is the number of unique edges  $K$ . For global statistics,  $R$  and  $C$  are both the total number of vertices  $N$ .

Following Rao et al. (2021), each self-attention mechanism is preceded by layer normalization and followed by dropout, with residual connections to the input,

$$x = x + \text{Dropout}(\text{Attn}(\text{LayerNorm}(x))). \quad (5)$$

We pass messages between the marginal and global layers to propagate information. Let  $\phi_{E,\ell}$  be marginal layer  $\ell$ , let  $\phi_{\rho,\ell}$  be global layer  $\ell$ , and let  $h^{\cdot,\ell}$  denote the hidden representations out of layer  $\ell$ . The marginal to global message  $m^{E \rightarrow \rho} \in \mathbb{R}^{N \times N \times d}$  contains representations of each edge averaged over subsets,

$$m_{i,j}^{E \rightarrow \rho, \ell} = \begin{cases} \frac{1}{T_e} \sum_t h_{t,e=(i,j)}^{E,\ell} & \text{if } \exists S_t, i, j \in S_t \\ \epsilon & \text{otherwise.} \end{cases} \quad (6)$$

where  $T_e$  is the number of  $S_t$  containing  $e$ , and missing entries are padded to learned constant  $\epsilon$ . The global to marginal message  $m^{\rho \rightarrow E} \in \mathbb{R}^{K \times d}$  is simply the hidden representation itself,

$$m_{t,e=(i,j)}^{\rho \rightarrow E, \ell} = h_{i,j}^{\rho, \ell}. \quad (7)$$

We update representations based on these messages as follows.

$$h^{E,\ell} = \phi_{E,\ell}(h^{E,\ell-1}) \quad (\text{marginal feature}) \quad (8)$$

$$h^{\rho,\ell-1} \leftarrow W^\ell [h^{\rho,\ell-1}, m^{E \rightarrow \rho, \ell}] \quad (\text{marginal to global}) \quad (9)$$

$$h^{\rho,\ell} = \phi_{\rho,\ell}(h^{\rho,\ell-1}) \quad (\text{global feature}) \quad (10)$$

$$h^{E,\ell} \leftarrow h^{E,\ell} + m^{\rho \rightarrow E, \ell} \quad (\text{global to marginal}) \quad (11)$$

$W^\ell \in \mathbb{R}^{2d \times d}$  is a learned linear projection, and  $[\cdot]$  denotes concatenation.

<sup>4</sup>The random permutation  $i' = \sigma(V)_i$  allows us to avoid updating positional embeddings of lower order positions more than higher order ones, due to the mixing of graph sizes during training.

**Graph prediction** For each pair of vertices  $i \neq j \in V$ , we predict  $e = 0, 1$ , or  $2$  for no edge,  $i \rightarrow j$ , and  $j \rightarrow i$ . We do not additionally enforce that our predicted graphs are acyclic, similar in spirit to Lippe et al. (2022). Given the output of the final axial attention block  $h^\rho$ , we compute logits

$$z_{\{i,j\}} = \text{FFN}([h_{i,j}^\rho, h_{j,i}^\rho]) \in \mathbb{R}^3 \quad (12)$$

which correspond to probabilities after softmax normalization. The overall output  $\hat{E} \in \{0, 1\}^{N \times N}$  is supervised by the ground truth  $E$ . Our model is trained with cross entropy loss and L2 regularization.

**Implementation details** Unless otherwise noted, inverse covariance is used for the global statistic and selection score, due to its relationship to partial correlation. We sample batches of size  $b = 500$  over  $k = 5$  nodes each (analysis in C.1). Our model was implemented with 4 layers with 8 attention heads and hidden dimension 64. Our model was trained using the AdamW optimizer with a learning rate of  $1e-4$  (Loshchilov & Hutter, 2019). See B.3 for additional details about hyperparameters.

**Complexity** The aggregator should be invariant to node labeling, while maintaining the order of sampled subsets, so attention-based architectures were a natural choice (Vaswani et al., 2017). If we concatenated  $\rho$  and  $E'_{1..T}$  into a length  $N^2T$  input, quadratic-scaling attention would cost  $O(N^4T^2)$ . Instead, we opted for axial attention blocks, which attend along each of the three axes separately in  $O(N^3T + N^2T^2)$ . Both are parallelizable on GPU, but the latter is more efficient.

### 3.4 Theoretical interpretation

**Marginal graph resolution** It is well-established that estimates of causal graphs over subsets of variables can be “merged” into consistent graphs over their union (Faller et al., 2023), and various algorithms have been proposed towards this task (Tillman et al., 2008; Huang et al., 2020a). Our main theoretical contribution is demonstrating that our axial attention model can implement such an algorithm under realistic conditions (description of algorithm and all proofs in Appendix A).

**Theorem 3.1.** *Let  $G = (V, E)$  be a directed acyclic graph with maximum degree  $d$ . For  $S \subseteq V$ , let  $E'_S$  denote the marginal estimate over  $S$ . Let  $\mathcal{S}_d$  denote the superset that contains all subsets  $S \subseteq V$  of size at most  $d$ . Given  $\{E'_S\}_{S \in \mathcal{S}_d}$ , a stack of  $L$  axial attention blocks has the capacity to recover  $G$ 's skeleton and  $v$ -structures in  $O(N)$  width, and propagate orientations on paths of  $O(L)$  length.*

There are two practical considerations that motivate a framework like SEA, instead of directly running these reconciliation algorithms. First, many of these algorithms rely on specific characterizations of the data-generating process, e.g. linear non-Gaussian (Huang et al., 2020a). While our proof does not constrain the causal mechanisms or exogenous noise, it assumes that the marginal estimates are correct. These assumptions may not hold on real data. However, the failure modes of causal discovery algorithms may be similar across datasets and can be corrected using statistics that capture richer information. For example, an algorithm that assumes linearity will make (predictably) asymmetric mistakes on non-linear data and underestimate the presence of edges. However, we may be able to recover nonlinear relationships with statistics like distance correlation (Sz'ekely et al., 2007). By training a deep learning model to reconcile marginal estimates and interpret global statistics, we are less sensitive to artifacts of sampling and discretization (e.g. p-value thresholds, statistics  $\leq 0$ ).

The second consideration is that checking a combinatorial number of subsets is wasteful on smaller graphs and infeasible on larger graphs. In fact, if we only leverage marginal estimates, we must check at least  $O(N^2)$  subsets to cover each edge at least once. To this end, the classical Independence Graph algorithm (Spirites et al., 2001) motivates statistics such as inverse covariance to initialize the undirected skeleton and reduce the number of independence tests required. This allows us to use marginal estimates more efficiently, towards answering orientation questions.

**On identifiability** The goal of this paper is a principled, yet practical framework for causal discovery. Instead of focusing on the identifiability of any particular setting, we offer the following interpretations of our model’s outputs. When all assumptions are upheld, and infinite data are available, the model has the capacity to infer a sound graph, as far as its (Markov/interventional) equivalence class. Given only observational data, the model will attempt to orient all edges, but the output can be interpreted as a member of the MEC. Given interventional data with sufficient interventions, the model should be able to identify the ground truth (Hauser & Bühlmann, 2012). When data do not match a causal discovery algorithm’s assumptions, its performance is inherently an empirical question. In this case, we show empirically that our model still does well (Section 5.1).

## 4 Experimental setup

We pretrained SEA models on diverse synthetic datasets. We evaluate on unseen in-distribution and out-of-distribution synthetic datasets, as well as two real biological datasets (Sachs et al., 2005; Replogle et al., 2022), using the versions from Wang et al. (2017); Chevalley et al. (2022). We also include experiments on simulated mRNA datasets in Appendix C.3 (Dibacina & Sinha, 2020). All baselines were trained and/or run from scratch on each testing dataset using their published code and hyperparameters, except AVICI (their recommended checkpoint was trained on their synthetic train and test sets after publication, Appendix B.2).

### 4.1 Synthetic data generation

The training datasets were constructed by 1) sampling Erdős-Rényi and scale free graphs with  $N = 10, 20, 100$  nodes and  $E = N, 2N, 3N, 4N$  expected edges; 2) sampling random instantiations of causal mechanisms (Linear, NN with additive/non-additive Gaussian noise); and 3) iteratively sampling observations in topological order (details in Appendix B.1). For each graph, we generated both observational and interventional datasets with  $1000N$  points, either all observational or split equally among observational and perfect single-node interventions. We generated 90 training, 5 validation, and 5 testing datasets for each combination (8160 total). For testing, we also sampled out-of-distribution datasets with 1) Sigmoid and Polynomial mechanisms (additive/non-additive Gaussian noise); and 2) Linear with additive non-Gaussian noise.

### 4.2 Causal discovery metrics

We report both discrete and continuous metrics, as neural networks can be notoriously uncalibrated (Guo et al., 2017), and arbitrary discretization thresholds reflect an incomplete picture (Schaeffer et al., 2023). Following previous work (Lorch et al., 2022), we compute metrics with respect to the ground truth graph. In the observational setting, the “oracle” expected value of each metric will vary depending on the size of the equivalence class (e.g. if multiple graphs are valid, their mean accuracy is  $< 1$  with respect to a single ground truth). For all continuous metrics, we exclude the diagonal since several baselines manually set it to zero (Brouillard et al., 2020; Lopez et al., 2022).

**SHD:** Structural Hamming distance is the minimum number of edge edits required to match two graphs (Tsamardinos et al., 2006). Discretization thresholds are as published or default to 0.5.

**mAP:** Mean average precision computes the area under precision-recall curve per edge and averages over the graph. The random guessing baseline depends on the positive rate.

**AUC:** Area under the ROC curve (Bradley, 1997) computed per edge (binary prediction) and averaged over the graph. For each edge, 0.5 indicates random guessing, while 1 indicates perfect performance.

**Orientation accuracy:** We compute the accuracy of edge orientations as

$$\text{OA} = \frac{\sum_{(i,j) \in E} \mathbb{1}\{P(i,j) > P(j,i)\}}{\|E\|}. \tag{13}$$

Since OA is normalized by  $\|E\|$ , it is invariant to the positive rate. In contrast to orientation F1 (Geffner et al., 2022), it is also invariant to the assignment of forward/reverse edges as 1/0.

### 4.3 Baselines

We compare against several deep learning and classical baselines. **DCDI** (Brouillard et al., 2020) extracts the causal graph as a parameter of a generative model. The G and DSF variants use Gaussian or deep sigmoidal flow likelihoods, respectively. **DCD-FG** (Lopez et al., 2022) follows DCDI-G, but factorizes the graph into a product of two low-rank matrices for scalability. **DIFFAN** (Sanchez et al., 2023) uses the trained model’s Hessian to obtain a topological ordering, followed by a classical pruning algorithm. **AVICI** (Lorch et al., 2022) uses an amortized inference approach to estimate  $P(G | D)$  over a class of data-generating mechanisms via variational inference. Both DCD-\* and AVICI were run with full knowledge of intervention targets.

**VARSORT** (Reisach et al., 2021) sorts nodes by marginal variance and sparsely regresses nodes based on their predecessors. This naive baseline is intended to reveal artifacts of synthetic data generation.

Table 1: Causal discovery results on synthetic datasets. Each setting encompasses 5 distinct Erdős-Rényi graphs (mAP stds all within 0.02). † indicates that this setting is o.o.d. \* indicates non-parametric bootstrapping. Runtimes based on 1 CPU and 1 V100 GPU. Baseline details in B.2.

$N$	$E$	Model	Linear		NN non-add.		Sigmoid†		Polynomial†		Overall
			mAP ↑	SHD ↓	Time(s) ↓						
10	10	DCDI-G	0.74	2.8	0.89	<b>1.0</b>	0.46	5.8	0.41	8.9	13425.4
		DCDI-DSF	0.82	2.0	0.50	4.2	0.38	6.3	0.29	11.2	11449.7
		DIFFAN	0.25	14.0	0.12	21.8	0.24	12.0	0.20	15.0	163.1
		AVICI	0.45	8.2	0.65	5.6	0.52	8.3	0.31	9.6	1.1
		VARSORT*	0.70	6.0	0.83	4.2	0.52	7.6	0.40	9.3	0.1
		FCI*	0.52	10.0	0.40	9.8	0.56	9.1	0.41	10.0	5.7
		GIES*	0.81	3.6	0.71	4.8	0.70	5.9	0.61	7.1	33.8
		SEA (FCI)	0.98	<b>1.0</b>	0.88	3.8	0.83	<b>3.9</b>	0.62	6.1	3.8
		SEA (GIES)	<b>0.99</b>	1.2	<b>0.91</b>	3.2	<b>0.85</b>	4.0	<b>0.70</b>	<b>5.8</b>	3.5
		20	80	DCDI-G	0.46	44.0	<b>0.82</b>	37.4	0.48	44.2	0.37
DCDI-DSF	0.48			41.2	0.74	<b>28.4</b>	0.48	43.6	0.38	57.6	11399.6
DIFFAN	0.21			127	0.18	145	0.22	117	0.18	157	558.0
AVICI	0.34			75.6	0.49	61.2	0.34	70.6	0.30	75.5	1.9
VARSORT*	0.76			44.8	0.47	65.2	0.59	63.4	0.38	75.6	0.3
FCI*	0.30			75.8	0.30	74.4	0.41	72.3	0.34	76.6	187.6
GIES*	0.41			70.0	0.46	67.4	0.50	65.6	0.49	68.1	814.3
SEA (FCI)	0.80			39.8	0.70	52.0	0.74	<b>42.9</b>	0.55	<b>57.0</b>	6.7
SEA (GIES)	<b>0.89</b>			<b>26.8</b>	0.73	50.6	<b>0.76</b>	45.0	<b>0.65</b>	60.1	4.3
100	400			DCD-FG	0.05	3068	0.10	3511	0.13	3602	0.12
		AVICI	0.12	392	0.23	382	0.10	399	0.03	402	7.8
		VARSORT*	0.80	225	0.34	355	0.51	350	0.27	380	6.7
		SEA (FCI)	0.84	162	0.52	339	0.63	247	0.34	<b>325</b>	18.6
		SEA (GIES)	<b>0.91</b>	<b>117</b>	<b>0.61</b>	<b>267</b>	<b>0.69</b>	<b>218</b>	<b>0.38</b>	328	3.7

**FCI, GIES** run the FCI and GIES algorithms over *all* nodes. VARSORT, FCI, and GIES were run using non-parametric bootstrapping (Friedman et al., 1999), with 100 subsets of 500 examples each.

## 5 Results

Our experiments cover two settings.

1. Section 5.1 examines the case where we have no prior knowledge about the data. Our models achieve high performance out-of-the-box, even when the data are misspecified or out-of-domain.
2. Section 5.2 focuses on the case where we do know (or can estimate) the class of causal mechanisms or exogenous noise. We show that adapting our pretrained models with this information (at low to zero additional training cost) leads to substantial improvement and exceeds the best baseline trained from scratch.

We highlight representative results towards each goal. Full results and ablations are in Appendix C, with additional metrics, baselines, hyperparameters, model components, and design choices.

### 5.1 Robustness and generalization

Table 1 summarizes our controlled experiments on synthetic data. SEA exceeds all baselines in the Linear, additive Gaussian case, which matches the models’ assumptions exactly (causal discovery algorithms and inverse covariance). In the misspecified (NN) or misspecified *and* out-of-distribution settings (Sigmoid, Polynomial), SEA also attains the best performance in the majority of cases, even though DCDI and AVICI both have access to the raw data. Furthermore, our models outperform

Table 2: Results on K562 single cell data, with STRING database (physical) as ground truth. Baselines taken from Chevalley et al. (2022).

Model	P $\uparrow$	R $\uparrow$	F1 $\uparrow$	Time(s) $\downarrow$
GRNBOOST	0.070	<b>0.710</b>	0.127	316
GIES	0.190	0.020	0.036	2350
NOTeARS	0.080	0.620	0.142	32883
DCDI-G	0.180	0.030	0.051	16561
DCDI-DSF	0.140	0.040	0.062	5709
DCD-FG	0.110	0.070	0.086	6368
SEA (G)+CORR with $b = 2000$	0.491	0.109	<b>0.179</b>	<b>4</b>
	<b>0.838</b>	0.093	0.167	5

Table 4: Adapting SEA to linear non-Gaussian (Uniform) noise. LINGAM run without finetuning; SEA(G) finetuned for distance correlation.

Model	N=10, E=10		N=20, E=20	
	mAP $\uparrow$	SHD $\downarrow$	mAP $\uparrow$	SHD $\downarrow$
DCDI-DSF	0.34	22.3	0.32	63.0
LINGAM*	0.34	7.2	0.30	18.8
SEA (G)	0.26	12.7	0.12	46.6
+LINGAM	0.52	10.1	0.22	39.7
+DCOR	0.44	8.0	0.21	33.1
+LING+DCOR	<b>0.76</b>	<b>4.6</b>	<b>0.67</b>	<b>14.2</b>

Table 3: Performance on Sachs (C.5) varies depending on implicit (AVICI training set) and explicit (SEA variants) assumptions.

Model	mAP $\uparrow$	AUC $\uparrow$	SHD $\downarrow$
DCDI-DSF	0.20	0.59	20.0
AVICI-L	0.35	0.78	20.0
AVICI-R	0.29	0.65	18.0
AVICI-L+R	<b>0.59</b>	<b>0.83</b>	14.0
SEA (F)	0.23	0.54	24.0
+KCI	0.33	0.63	14.0
+CORR	0.41	0.70	15.0
+KCI+CORR	0.49	0.71	<b>13.0</b>

Table 5: Adapting SEA to polynomial, sigmoid non-additive (N=10, E=10). FCI run with KCI test; SEA(F) finetuned for distance correlation.

Model	Polynomial		Sigmoid	
	mAP $\uparrow$	SHD $\downarrow$	mAP $\uparrow$	SHD $\downarrow$
DCDI-DSF	0.39	9.8	0.81	13.6
FCI*	0.12	10.6	0.53	8.1
SEA (F)	0.22	10.6	0.59	4.8
+KCI	0.30	10.6	0.59	5.5
+DCOR	0.45	9.6	<b>0.90</b>	<b>2.1</b>
+KCI+DCOR	<b>0.52</b>	<b>8.2</b>	0.86	3.4

VARSORT in every single setting, while most baselines are unable to do so consistently. This indicates that our models do not simply overfit to spurious features of the synthetic data generation process.

Table 2 illustrates that we exceed baselines on single cell gene expression data from Causal-Bench (Chevalley et al., 2022; Replogle et al., 2022). Furthermore, when we increase the subset size to  $b = 2000$ , we achieve very high precision (0.838) over 2834 predicted edges. SEA runs within 5s on this dataset of 162k cells and  $N = 622$  genes, while the fastest naive baseline takes 5 minutes and the slowest deep learning baseline takes 9 hours (run in parallel on subsets of genes).

## 5.2 Low-cost adaptation

We illustrate two strategies that allow us to use pretrained SEA models with different implicit assumptions. First, if two causal discovery algorithms share the same output format, they can be used interchangeably for marginal estimation (though there may be a performance drop if the mistakes themselves are out of distribution). On observational, linear non-Gaussian data, replacing the GES algorithm with LINGAM (Shimizu et al., 2006) is beneficial without any other change (Table 4). The same effect can be observed on Polynomial and Sigmoid non-additive data, when running FCI with a polynomial kernel conditional independence test (Zhang et al., 2011) instead of the Fisherz test (Table 5). Second, we may “finetune” the aggregator using low-cost methods like LoRA (Hu et al., 2022). Specifically, we keep the same training set and objective, and change the global statistic (or discovery algorithm). Here, we show that finetuning our models for distance correlation is beneficial in both cases, and the combination of strategies results in the highest performance overall, surpassing the best baseline trained from scratch (DCDI-DSF).

On real data from unknown data-generating processes, the ability to run causal discovery with different assumptions is useful when coupled with unsupervised methods for model selection (Faller et al., 2023). Table 3 illustrates two such approaches for continuous optimization algorithms. Methods like AVICI, which operate on raw data, must re-train/finetune the model on the expanded data (around

4 days). In contrast, SEA can be run directly with a different estimation algorithm, or finetuned on the same data for around 4-6 hours (1 A6000) and  $< 4$  GB of GPU memory.

### **5.3 Limitations**

Some empirical limitations of our implementations include: 1) a hard-coded maximum of 1000 variables (arbitrary), 2) generalize poorly to synthetic cyclic data, 3) err on the side of sparsity on real data, 4) inverse covariance can be numerically unstable on larger graphs (recommend models finetuned for correlation here), and 5) training requires full precision. These can be seen as artifacts of our training set and design choices.

### **Acknowledgements**

We thank Bowen Jing, Felix Faltings, Sean Murphy, and Wenxian Shi for helpful discussions regarding the writing; as well as Jiaqi Zhang, Romain Lopez, Caroline Uhler, and Stephen Bates for helpful feedback regarding the framing of this project.

This material is based upon work supported by the National Science Foundation Graduate Research Fellowship under Grant No. 1745302. We would like to acknowledge support from the NSF Expeditions grant (award 1918839: Collaborative Research: Understanding the World Through Code), Machine Learning for Pharmaceutical Discovery and Synthesis (MLPDS) consortium, and the Abdul Latif Jameel Clinic for Machine Learning in Health.

## References

- Steen A. Andersson, David Madigan, and Michael D. Perlman. A characterization of Markov equivalence classes for acyclic digraphs. *The Annals of Statistics*, 25(2):505 – 541, 1997. doi: 10.1214/aos/1031833662.
- Rishi Bommasani, Drew A. Hudson, Ehsan Adeli, Russ Altman, Simran Arora, Sydney von Arx, Michael S. Bernstein, Jeannette Bohg, Antoine Bosselut, Emma Brunskill, Erik Brynjolfsson, Shyamal Buch, Dallas Card, Rodrigo Castellon, Niladri Chatterji, Annie Chen, Kathleen Creel, Jared Quincy Davis, Dora Demszky, Chris Donahue, Moussa Doumbouya, Esin Durmus, Stefano Ermon, John Etchemendy, Kawin Ethayarajh, Li Fei-Fei, Chelsea Finn, Trevor Gale, Lauren Gillespie, Karan Goel, Noah Goodman, Shelby Grossman, Neel Guha, Tatsunori Hashimoto, Peter Henderson, John Hewitt, Daniel E. Ho, Jenny Hong, Kyle Hsu, Jing Huang, Thomas Icard, Saahil Jain, Dan Jurafsky, Pratyusha Kalluri, Siddharth Karamcheti, Geoff Keeling, Fereshte Khani, Omar Khattab, Pang Wei Koh, Mark Krass, Ranjay Krishna, Rohith Kuditipudi, Ananya Kumar, Faisal Ladhak, Mina Lee, Tony Lee, Jure Leskovec, Isabelle Levent, Xiang Lisa Li, Xuechen Li, Tengyu Ma, Ali Malik, Christopher D. Manning, Suvir Mirchandani, Eric Mitchell, Zanele Munyikwa, Suraj Nair, Avani Narayan, Deepak Narayanan, Ben Newman, Allen Nie, Juan Carlos Niebles, Hamed Nilforoshan, Julian Nyarko, Giray Ogut, Laurel Orr, Isabel Papadimitriou, Joon Sung Park, Chris Piech, Eva Portelance, Christopher Potts, Aditi Raghunathan, Rob Reich, Hongyu Ren, Frieda Rong, Yusuf Roohani, Camilo Ruiz, Jack Ryan, Christopher Ré, Dorsa Sadigh, Shiori Sagawa, Keshav Santhanam, Andy Shih, Krishnan Srinivasan, Alex Tamkin, Rohan Taori, Armin W. Thomas, Florian Tramèr, Rose E. Wang, William Wang, Bohan Wu, Jiajun Wu, Yuhuai Wu, Sang Michael Xie, Michihiro Yasunaga, Jiaxuan You, Matei Zaharia, Michael Zhang, Tianyi Zhang, Xikun Zhang, Yuhui Zhang, Lucia Zheng, Kaitlyn Zhou, and Percy Liang. On the opportunities and risks of foundation models, 2022.
- Andrew P. Bradley. The use of the area under the roc curve in the evaluation of machine learning algorithms. *Pattern Recognition*, 30(7):1145–1159, 1997. ISSN 0031-3203. doi: [https://doi.org/10.1016/S0031-3203\(96\)00142-2](https://doi.org/10.1016/S0031-3203(96)00142-2).
- Philippe Brouillard, Sébastien Lachapelle, Alexandre Lacoste, Simon Lacoste-Julien, and Alexandre Drouin. Differentiable causal discovery from interventional data, 2020.
- Tom B. Brown, Benjamin Mann, Nick Ryder, Melanie Subbiah, Jared Kaplan, Prafulla Dhariwal, Arvind Neelakantan, Pranav Shyam, Girish Sastry, Amanda Askell, Sandhini Agarwal, Ariel Herbert-Voss, Gretchen Krueger, Tom Henighan, Rewon Child, Aditya Ramesh, Daniel M. Ziegler, Jeffrey Wu, Clemens Winter, Christopher Hesse, Mark Chen, Eric Sigler, Mateusz Litwin, Scott Gray, Benjamin Chess, Jack Clark, Christopher Berner, Sam McCandlish, Alec Radford, Ilya Sutskever, and Dario Amodei. Language models are few-shot learners, 2020.
- Peter Bühlmann, Jonas Peters, and Jan Ernest. CAM: Causal additive models, high-dimensional order search and penalized regression. *The Annals of Statistics*, 42(6):2526 – 2556, 2014. doi: 10.1214/14-AOS1260.
- Mathieu Chevalley, Yusuf Roohani, Arash Mehrjou, Jure Leskovec, and Patrick Schwab. CausalBench: A Large-scale Benchmark for Network Inference from Single-cell Perturbation Data. *arXiv preprint arXiv:2210.17283*, 2022.
- David Maxwell Chickering. Optimal structure identification with greedy search. 3:507–554, November 2002.
- Payam Dibaeinia and Saurabh Sinha. Sergio: A single-cell expression simulator guided by gene regulatory networks. *Cell Systems*, 11(3):252–271.e11, 2020. ISSN 2405-4712. doi: <https://doi.org/10.1016/j.cels.2020.08.003>.
- Philipp M. Faller, Leena Chennuru Vankadara, Atalanti A. Mastakouri, Francesco Locatello, Dominik Janzing Karlsruhe Institute of Technology, and Amazon Research Tuebingen. Self-compatibility: Evaluating causal discovery without ground truth. *International Conference on Artificial Intelligence and Statistics*, 2023.

- Nir Friedman, Moisés Goldszmidt, and Abraham J. Wyner. Data analysis with bayesian networks: A bootstrap approach. *Proceedings of the Fifteenth Conference on Uncertainty in Artificial Intelligence, UAI'99*, pp. 196–205, 1999.
- Tomas Geffner, Javier Antoran, Adam Foster, Wenbo Gong, Chao Ma, Emre Kiciman, Amit Sharma, Angus Lamb, Martin Kukla, Nick Pawlowski, Miltiadis Allamanis, and Cheng Zhang. Deep end-to-end causal inference, 2022.
- Clark Glymour, Kun Zhang, and Peter Spirtes. Review of causal discovery methods based on graphical models. *Frontiers in Genetics*, 10, 2019. ISSN 1664-8021. doi: 10.3389/fgene.2019.00524.
- Chuan Guo, Geoff Pleiss, Yu Sun, and Kilian Q. Weinberger. On calibration of modern neural networks. In *International Conference on Machine Learning*, 2017.
- Alain Hauser and Peter Bühlmann. Characterization and greedy learning of interventional markov equivalence classes of directed acyclic graphs. *Journal of Machine Learning Research*, 13(79): 2409–2464, 2012.
- Alain Hauser and Peter Bühlmann. Characterization and greedy learning of interventional markov equivalence classes of directed acyclic graphs. 2012.
- Jonathan Ho, Nal Kalchbrenner, Dirk Weissenborn, and Tim Salimans. Axial attention in multidimensional transformers, 2020.
- Kurt Hornik, Maxwell Stinchcombe, and Halbert White. Multilayer feedforward networks are universal approximators. *Neural Networks*, 2(5):359–366, 1989. ISSN 0893-6080. doi: [https://doi.org/10.1016/0893-6080\(89\)90020-8](https://doi.org/10.1016/0893-6080(89)90020-8).
- Edward J Hu, yelong shen, Phillip Wallis, Zeyuan Allen-Zhu, Yuanzhi Li, Shean Wang, Lu Wang, and Weizhu Chen. LoRA: Low-rank adaptation of large language models. In *International Conference on Learning Representations*, 2022. URL <https://openreview.net/forum?id=nZeVKeeFYf9>.
- Biwei Huang, Kun Zhang, Mingming Gong, and Clark Glymour. Causal discovery from multiple data sets with non-identical variable sets. *Proceedings of the AAAI Conference on Artificial Intelligence*, 34(06):10153–10161, Apr. 2020a. doi: 10.1609/aaai.v34i06.6575.
- Biwei Huang, Kun Zhang, Jiji Zhang, Joseph Ramsey, Ruben Sanchez-Romero, Clark Glymour, and Bernhard Schölkopf. Causal discovery from heterogeneous/nonstationary data with independent changes, 2020b.
- Diviyani Kalainathan, Olivier Goudet, and Ritik Dutta. Causal discovery toolbox: Uncovering causal relationships in python. *Journal of Machine Learning Research*, 21(37):1–5, 2020.
- Nan Rosemary Ke, Silvia Chiappa, Jane Wang, Anirudh Goyal, Jorg Bornschein, Melanie Rey, Theophane Weber, Matthew Botvinic, Michael Mozer, and Danilo Jimenez Rezende. Learning to induce causal structure, 2022.
- Sébastien Lachapelle, Philippe Brouillard, Tristan Deleu, and Simon Lacoste-Julien. Gradient-based neural dag learning, 2020.
- Wai-Yin Lam, Bryan Andrews, and Joseph Ramsey. Greedy relaxations of the sparsest permutation algorithm. In James Cussens and Kun Zhang (eds.), *Proceedings of the Thirty-Eighth Conference on Uncertainty in Artificial Intelligence*, volume 180 of *Proceedings of Machine Learning Research*, pp. 1052–1062. PMLR, 01–05 Aug 2022.
- Olivier Ledoit and Michael Wolf. A well-conditioned estimator for large-dimensional covariance matrices. *Journal of Multivariate Analysis*, 88(2):365–411, 2004. ISSN 0047-259X. doi: [https://doi.org/10.1016/S0047-259X\(03\)00096-4](https://doi.org/10.1016/S0047-259X(03)00096-4).
- Phillip Lippe, Taco Cohen, and Efstratios Gavves. Efficient neural causal discovery without acyclicity constraints. In *International Conference on Learning Representations*, 2022.

- Romain Lopez, Jan-Christian Hütter, Jonathan K. Pritchard, and Aviv Regev. Large-scale differentiable causal discovery of factor graphs. In *Advances in Neural Information Processing Systems*, 2022.
- Lars Lorch, Scott Sussex, Jonas Rothfuss, Andreas Krause, and Bernhard Schölkopf. Amortized inference for causal structure learning, 2022.
- Ilya Loshchilov and Frank Hutter. Decoupled weight decay regularization, 2019.
- Sindy Löwe, David Madras, Richard Zemel, and Max Welling. Amortized causal discovery: Learning to infer causal graphs from time-series data, 2022.
- Ricardo Pio Monti, Kun Zhang, and Aapo Hyvarinen. Causal discovery with general non-linear relationships using non-linear ica, 2019.
- Joris M. Mooij, Sara Magliacane, and Tom Claassen. Joint causal inference from multiple contexts. 2020.
- Jorge Pérez, Javier Marinković, and Pablo Barceló. On the turing completeness of modern neural network architectures. In *International Conference on Learning Representations*, 2019.
- Alec Radford, Jong Wook Kim, Chris Hallacy, Aditya Ramesh, Gabriel Goh, Sandhini Agarwal, Girish Sastry, Amanda Askell, Pamela Mishkin, Jack Clark, Gretchen Krueger, and Ilya Sutskever. Learning transferable visual models from natural language supervision, 2021.
- Roshan M Rao, Jason Liu, Robert Verkuil, Joshua Meier, John Canny, Pieter Abbeel, Tom Sercu, and Alexander Rives. Msa transformer. In Marina Meila and Tong Zhang (eds.), *Proceedings of the 38th International Conference on Machine Learning*, volume 139 of *Proceedings of Machine Learning Research*, pp. 8844–8856. PMLR, 18–24 Jul 2021.
- Alexander G. Reisach, Christof Seiler, and Sebastian Weichwald. Beware of the simulated dag! causal discovery benchmarks may be easy to game. *Advances in Neural Information Processing Systems*, 34, 2021.
- Patrik Reizinger, Yash Sharma, Matthias Bethge, Bernhard Schölkopf, Ferenc Huszár, and Wieland Brendel. Jacobian-based causal discovery with nonlinear ICA. *Transactions on Machine Learning Research*, 2023. ISSN 2835-8856.
- J. M. Replogle, R. A. Saunders, A. N. Pogson, J. A. Hussmann, A. Lenail, A. Guna, L. Mascibroda, E. J. Wagner, K. Adelman, G. Lithwick-Yanai, N. Iremadze, F. Oberstrass, D. Lipson, J. L. Bonnar, M. Jost, T. M. Norman, and J. S. Weissman. Mapping information-rich genotype-phenotype landscapes with genome-scale Perturb-seq. *Cell*, 185(14):2559–2575, Jul 2022.
- Karen Sachs, Omar Perez, Dana Pe’er, Douglas A. Lauffenburger, and Garry P. Nolan. Causal protein-signaling networks derived from multiparameter single-cell data. *Science*, 308(5721): 523–529, 2005. doi: 10.1126/science.1105809.
- Pedro Sanchez, Xiao Liu, Alison Q. O’Neil, and Sotirios A. Tsafaris. Diffusion models for causal discovery via topological ordering. In *The Eleventh International Conference on Learning Representations, ICLR 2023, Kigali, Rwanda, May 1-5, 2023*. OpenReview.net, 2023.
- Rylan Schaeffer, Brando Miranda, and Oluwasanmi Koyejo. Are emergent abilities of large language models a mirage? *Advances in Neural Information Processing Systems*, abs/2304.15004, 2023.
- Gideon Schwarz. Estimating the Dimension of a Model. *The Annals of Statistics*, 6(2):461 – 464, 1978. doi: 10.1214/aos/1176344136.
- Shohei Shimizu, Patrik O. Hoyer, Aapo Hyvarinen, and Antti Kerminen. A linear non-gaussian acyclic model for causal discovery. *Journal of Machine Learning Research*, 7(72):2003–2030, 2006.
- Peter Spirtes, Clark Glymour, and Richard Scheines. Causality from probability. In *Conference Proceedings: Advanced Computing for the Social Sciences*, 1990.

- Peter Spirtes, Christopher Meek, and Thomas Richardson. Causal inference in the presence of latent variables and selection bias. In *Proceedings of the Eleventh Conference on Uncertainty in Artificial Intelligence, UAI'95*, pp. 499–506, San Francisco, CA, USA, 1995. Morgan Kaufmann Publishers Inc. ISBN 1558603859.
- Peter Spirtes, Clark Glymour, and Richard Scheines. *Causation, Prediction, and Search*. MIT Press, 2001. doi: <https://doi.org/10.7551/mitpress/1754.001.0001>.
- G'abor J. Sz'ekely, Maria L. Rizzo, and Nail K. Bakirov. Measuring and testing dependence by correlation of distances. *Annals of Statistics*, 35:2769–2794, 2007.
- Robert Tillman, David Danks, and Clark Glymour. Integrating locally learned causal structures with overlapping variables. volume 21, pp. 1665–1672, 01 2008.
- Ioannis Tsamardinos, Laura E Brown, and Constantin F Aliferis. The max-min hill-climbing bayesian network structure learning algorithm. *Machine learning*, 65(1):31–78, 2006.
- Ashish Vaswani, Noam Shazeer, Niki Parmar, Jakob Uszkoreit, Llion Jones, Aidan N Gomez, Ł ukasz Kaiser, and Illia Polosukhin. Attention is all you need. In I. Guyon, U. Von Luxburg, S. Bengio, H. Wallach, R. Fergus, S. Vishwanathan, and R. Garnett (eds.), *Advances in Neural Information Processing Systems*, volume 30. Curran Associates, Inc., 2017.
- Tom S. Verma and Judea Pearl. On the equivalence of causal models. In *Proceedings of the Sixth Conference on Uncertainty in Artificial Intelligence*, 1990.
- Yuhao Wang, Liam Solus, Karren Yang, and Caroline Uhler. Permutation-based causal inference algorithms with interventions. In I. Guyon, U. Von Luxburg, S. Bengio, H. Wallach, R. Fergus, S. Vishwanathan, and R. Garnett (eds.), *Advances in Neural Information Processing Systems*, volume 30. Curran Associates, Inc., 2017.
- Chulhee Yun, Srinadh Bhojanapalli, Ankit Singh Rawat, Sashank J. Reddi, and Sanjiv Kumar. Are transformers universal approximators of sequence-to-sequence functions? *CoRR*, abs/1912.10077, 2019.
- Kun Zhang and Aapo Hyvarinen. On the identifiability of the post-nonlinear causal model, 2012.
- Kun Zhang, J. Peters, Dominik Janzing, and Bernhard Scholkopf. Kernel-based conditional independence test and application in causal discovery. *Conference on Uncertainty in Artificial Intelligence*, 2011.
- Xun Zheng, Bryon Aragam, Pradeep Ravikumar, and Eric P. Xing. Dags with no tears: Continuous optimization for structure learning, 2018.
- Yujia Zheng, Biwei Huang, Wei Chen, Joseph Ramsey, Mingming Gong, Ruichu Cai, Shohei Shimizu, Peter Spirtes, and Kun Zhang. Causal-learn: Causal discovery in python. *arXiv preprint arXiv:2307.16405*, 2023.

## A Proofs and derivations

Our theoretical contributions focus on two primary directions.

1. We formalize the notion of marginal estimates used in this paper, and prove that given sufficient marginal estimates, it is possible to recover a pattern faithful to the global causal graph. We provide lower bounds on the number of marginal estimates required for such a task, and motivate global statistics as an efficient means to reduce this bound.
2. We show that our proposed axial attention has the capacity to recapitulate the reasoning required for marginal estimate resolution. We provide realistic, finite bounds on the width and depth required for this task.

Before these formal discussions, we start with a toy example to provide intuition regarding marginal estimates and constraint-based causal discovery algorithms.

### A.1 Toy example: Resolving marginal graphs

Consider the Y-shaped graph with four nodes in Figure 3. Suppose we run the PC algorithm on all subsets of three nodes, and we would like to recover the result of the PC algorithm on the full graph. We illustrate how one might resolve the marginal graph estimates. The PC algorithm consists of the following steps (Spirtes et al., 2001).

1. Start from the fully connected, undirected graph on  $N$  nodes.
2. Remove all edges  $(i, j)$  where  $X_i \perp\!\!\!\perp X_j$ .
3. For each edge  $(i, j)$  and subsets  $S \subseteq [N] \setminus \{i, j\}$  of increasing size  $n = 1, 2, \dots, d$ , where  $d$  is the maximum degree in  $G$ , and all  $k \in S$  are connected to either  $i$  or  $j$ : if  $X_i \perp\!\!\!\perp X_j \mid S$ , remove edge  $(i, j)$ .
4. For each triplet  $(i, j, k)$ , such that only edges  $(i, k)$  and  $(j, k)$  remain, if  $k$  was not in the set  $S$  that eliminated edge  $(i, j)$ , then orient the “v-structure” as  $i \rightarrow k \leftarrow j$ .
5. (Orientation propagation) If  $i \rightarrow j$ , edge  $(j, k)$  remains, and edge  $(i, k)$  has been removed, orient  $j \rightarrow k$ . If there is a directed path  $i \rightsquigarrow j$  and an undirected edge  $(i, j)$ , then orient  $i \rightarrow j$ .

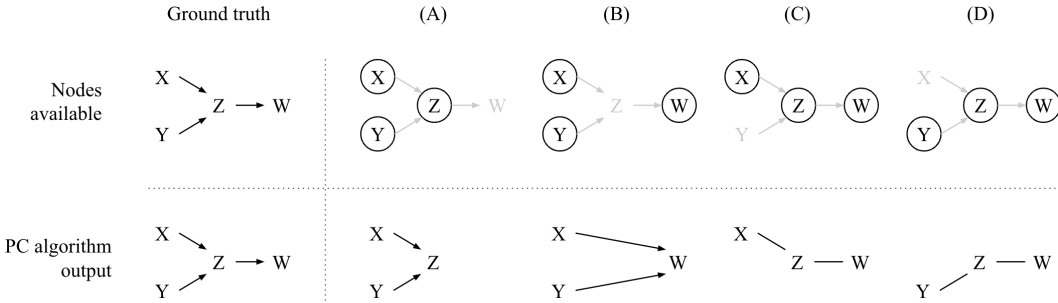


Figure 3: Resolving marginal graphs. Subsets of nodes revealed to the PC algorithm (circled in row 1) and its outputs (row 2).

In each of the four cases, the PC algorithm estimates the respective graphs as follows.

- (A) We remove edge  $(X, Y)$  via (2) and orient the v-structure.
- (B) We remove edge  $(X, Y)$  via (2) and orient the v-structure.
- (C) We remove edge  $(X, W)$  via (3) by conditioning on  $Z$ . There are no v-structures, so the edges remain undirected.
- (D) We remove edge  $(Y, W)$  via (3) by conditioning on  $Z$ . There are no v-structures, so the edges remain undirected.

The outputs (A-D) admit the full PC algorithm output as the only consistent graph on four nodes.

- $X$  and  $Y$  are unconditionally independent, so no subset will reveal an edge between  $(X, Y)$ .
- There are no edges between  $(X, W)$  and  $(Y, W)$ . Otherwise, (C) and (D) would yield the undirected triangle.

- $X, Y, Z$  must be oriented as  $X \rightarrow Z \leftarrow Y$ . Paths  $X \rightarrow Z \rightarrow Y$  and  $X \leftarrow Z \leftarrow Y$  would induce an  $(X, Y)$  edge in (B). Reversing orientations  $X \leftarrow Z \rightarrow Y$  would contradict (A).
- $(Y, Z)$  must be oriented as  $Y \rightarrow Z$ . Otherwise, (A) would remain unoriented.

## A.2 Resolving marginal estimates into global graphs

Classical results have characterized the Markov equivalency class of directed acyclic graphs. Two graphs are observationally equivalent if they have the same skeleton and v-structures (Verma & Pearl, 1990). Thus, a pattern  $P$  is *faithful* to a graph  $G$  if and only if they share the same skeletons and v-structures (Spirtes et al., 1990).

**Definition A.1.** Let  $G = (V, E)$  be a directed acyclic graph. A *pattern*  $P$  is a set of directed and undirected edges over  $V$ .

**Definition A.2** (Theorem 3.4 from Spirtes et al. (2001)). If pattern  $P$  is *faithful* to some directed acyclic graph, then  $P$  is faithful to  $G$  if and only if

1. for all vertices  $X, Y$  of  $G$ ,  $X$  and  $Y$  are adjacent if and only if  $X$  and  $Y$  are dependent conditional on every set of vertices of  $G$  that does not include  $X$  or  $Y$ ; and
2. for all vertices  $X, Y, Z$ , such that  $X$  is adjacent to  $Y$  and  $Y$  is adjacent to  $Z$  and  $X$  and  $Z$  are not adjacent,  $X \rightarrow Y \leftarrow Z$  is a subgraph of  $G$  if and only if  $X, Z$  are dependent conditional on every set containing  $Y$  but not  $X$  or  $Z$ .

Given data faithful to  $G$ , a number of classical constraint-based algorithms produce patterns that are faithful to  $G$ . We denote this set of algorithms as  $\mathcal{F}$ .

**Theorem A.3** (Theorem 5.1 from Spirtes et al. (2001)). *If the input to the PC, SGS, PC-1, PC-2, PC\*, or IG algorithms faithful to directed acyclic graph  $G$ , the output is a pattern that represents the faithful indistinguishability class of  $G$ .*

The algorithms in  $\mathcal{F}$  are sound and complete *if* there are no unobserved confounders.

Let  $P_V$  be a probability distribution that is Markov, minimal, and faithful to  $G$ . Let  $D \in \mathbb{R}^{M \times N} \sim P_V$  be a dataset of  $M$  observations over all  $N = |V|$  nodes.

Consider a subset  $S \subseteq V$ . Let  $D[S]$  denote the subset of  $D$  over  $S$ ,

$$D[S] = \{x_{i,v} : v \in S\}_{i=1}^N, \quad (14)$$

and let  $G[S]$  denote the subgraph of  $G$  induced by  $S$

$$G[S] = (S, \{(i, j) : i, j \in S, (i, j) \in E\}). \quad (15)$$

If we apply any  $f \in \mathcal{F}$  to  $D[S]$ , the results are *not* necessarily faithful to  $G[S]$ , as now there may be latent confounders in  $V \setminus S$  (by construction). We introduce the term *marginal estimate* to denote the resultant pattern that, while not faithful to  $G[S]$ , is still informative.

**Definition A.4** (Marginal estimate). A pattern  $E'$  is a *marginal estimate* of  $G[S]$  if and only if

1. for all vertices  $X, Y$  of  $S$ ,  $X$  and  $Y$  are adjacent if and only if  $X$  and  $Y$  are dependent conditional on every set of vertices of  $S$  that does not include  $X$  or  $Y$ ; and
2. for all vertices  $X, Y, Z$ , such that  $X$  is adjacent to  $Y$  and  $Y$  is adjacent to  $Z$  and  $X$  and  $Z$  are not adjacent,  $X \rightarrow Y \leftarrow Z$  is a subgraph of  $S$  if and only if  $X, Z$  are dependent conditional on every set containing  $Y$  but not  $X$  or  $Z$ .

**Proposition A.5.** *Let  $G = (V, E)$  be a directed acyclic graph with maximum degree  $d$ . For  $S \subseteq V$ , let  $E'_S$  denote the marginal estimate over  $S$ . Let  $\mathcal{S}_d$  denote the superset that contains all subsets  $S \subseteq V$  of size at most  $d$ . Algorithm 1 maps  $\{E'_S\}_{S \in \mathcal{S}_d}$  to a pattern  $E'$  faithful to  $G$ .*

On a high level, lines 3-8 recover the undirected “skeleton” graph of  $E^*$ , lines 9-15 recover the v-structures, and line 16 references step 5 in Section A.1.

*Remark A.6.* In the PC algorithm (Spirtes et al. (2001), A.1), its derivatives, and Algorithm 1, there is no need to consider separating sets with cardinality greater than maximum degree  $d$ , since the maximum number of independence tests required to separate any node from the rest of the graph is equal to number of its parents plus its children (due to the Markov assumption).

---

**Algorithm 1** Resolve marginal estimates of  $f \in \mathcal{F}$ 


---

```

1: Input: Data  $\mathcal{D}_G$  faithful to  $G$ 
2: Initialize  $E' \leftarrow K_N$  as the complete undirected graph on  $N$  nodes.
3: for  $S \in \mathcal{S}_{d+2}$  do
4:   Compute  $E'_S = f(\mathcal{D}_{G[S]})$ 
5:   for  $(i, j) \notin E'_S$  do
6:     Remove  $(i, j)$  from  $E'$ 
7:   end for
8: end for
9: for  $E'_S \in \{E'_S\}_{\mathcal{S}_{d+2}}$  do
10:  for v-structure  $i \rightarrow j \leftarrow k$  in  $E'_S$  do
11:    if  $\{i, j\}, \{j, k\} \in E'$  and  $\{i, k\} \notin E'$  then
12:      Assign orientation  $i \rightarrow j \leftarrow k$  in  $E'$ 
13:    end if
14:  end for
15: end for
16: Propagate orientations in  $E'$  (optional).

```

---

**Lemma A.7.** *The undirected skeleton of  $E^*$  is equivalent to the undirected skeleton of  $E'$*

$$C^* := \{\{i, j\} \mid (i, j) \in E^* \text{ or } (j, i) \in E^*\} = \{\{i, j\} \mid (i, j) \in E' \text{ or } (j, i) \in E'\} := C'. \quad (16)$$

That is,  $\{i, j\} \in C^* \iff \{i, j\} \in C'$ .

*Proof.* It is equivalent to show that  $\{i, j\} \notin C^* \iff \{i, j\} \notin C'$

$\Rightarrow$  If  $\{i, j\} \notin C^*$ , then there must exist a separating set  $S$  in  $G$  of at most size  $d$  such that  $i \perp\!\!\!\perp j \mid S$ . Then  $S \cup \{i, j\}$  is a set of at most size  $d + 2$ , where  $\{i, j\} \notin C'_{S \cup \{i, j\}}$ . Thus,  $\{i, j\}$  would have been removed from  $C'$  in line 6 of Algorithm 1.

$\Leftarrow$  If  $\{i, j\} \notin C'$ , let  $S$  be a separating set in  $\mathcal{S}_{d+2}$  such that  $\{i, j\} \notin C'_{S \cup \{i, j\}}$  and  $i \perp\!\!\!\perp j \mid S$ .  $S$  is also a separating set in  $G$ , and conditioning on  $S$  removes  $\{i, j\}$  from  $C^*$ .  $\square$

**Lemma A.8.** *A v-structure  $i \rightarrow j \leftarrow k$  exists in  $E^*$  if and only if there exists the same v-structure in  $E'$ .*

*Proof.* The PCI algorithm orients v-structures  $i \rightarrow j \leftarrow k$  in  $E^*$  if there is an edge between  $\{i, j\}$  and  $\{j, k\}$  but not  $\{i, k\}$ ; and if  $j$  was not in the conditioning set that removed  $\{i, k\}$ . Algorithm 1 orients v-structures  $i \rightarrow j \leftarrow k$  in  $E'$  if they are oriented as such in any  $E'_S$ ; and if  $\{i, j\}, \{j, k\} \in E'$ ,  $\{i, k\} \notin E'$

$\Rightarrow$  Suppose for contradiction that  $i \rightarrow j \leftarrow k$  is oriented as a v-structure in  $E^*$ , but not in  $E'$ . There are two cases.

1. No  $E'_S$  contains the undirected path  $i - j - k$ . If either  $i - j$  or  $j - k$  are missing from any  $E'_S$ , then  $E^*$  would not contain  $(i, j)$  or  $(k, j)$ . Otherwise, if all  $S$  contain  $\{i, k\}$ , then  $E^*$  would not be missing  $\{i, k\}$  (Lemma A.7).
2. In every  $E'_S$  that contains  $i - j - k$ ,  $j$  is in the conditioning set that removed  $\{i, k\}$ , i.e.  $i \perp\!\!\!\perp k \mid S, S \ni j$ . This would violate the faithfulness property, as  $j$  is neither a parent of  $i$  or  $k$  in  $E^*$ , and the outputs of the PC algorithm are faithful to the equivalence class of  $G$  (Theorem 5.1 Spirtes et al. (2001)).

$\Leftarrow$  Suppose for contradiction that  $i \rightarrow j \leftarrow k$  is oriented as a v-structure in  $E'$ , but not in  $E^*$ . By Lemma A.7, the path  $i - j - k$  must exist in  $E^*$ . There are two cases.

1. If  $i \rightarrow j \rightarrow k$  or  $i \leftarrow j \leftarrow k$ , then  $j$  must be in the conditioning set that removes  $\{i, k\}$ , so no  $E'_S$  containing  $\{i, j, k\}$  would orient them as v-structures.
2. If  $j$  is the root of a fork  $i \leftarrow j \rightarrow k$ , then as the parent of both  $i$  and  $k$ ,  $j$  must be in the conditioning set that removes  $\{i, k\}$ , so no  $E'_S$  containing  $\{i, j, k\}$  would orient them as v-structures.

Therefore, all v-structures in  $E'$  are also v-structures in  $E^*$ .  $\square$

*Proof of Proposition A.5.* Given data that is faithful to  $G$ , Algorithm 1 produces a pattern  $E'$  with the same connectivity and v-structures as  $E^*$ . Any additional orientations in both patterns are propagated using identical, deterministic procedures, so  $E' = E^*$ .  $\square$

This proof presents a deterministic but inefficient algorithm for resolving marginal subgraph estimates. In reality, it is possible to recover the undirected skeleton and the v-structures of  $G$  without checking all subsets  $S \in \mathcal{S}_{d+2}$ .

**Proposition A.9** (Skeleton bounds). *Let  $G = (V, E)$  be a directed acyclic graph with maximum degree  $d$ . It takes  $O(N^2)$  marginal estimates over subsets of size  $d + 2$  to recover the undirected skeleton of  $G$ .*

*Proof.* Following Lemma A.7, an edge  $(i, j)$  is not present in  $C$  if it is not present in any of the size  $d + 2$  estimates. Therefore, every pair of nodes  $\{i, j\}$  requires only a single estimate of size  $d + 2$ , so it is possible to recover  $C$  in  $\binom{N}{2}$  estimates.  $\square$

**Proposition A.10** (V-structures bounds). *Let  $G = (V, E)$  be a directed acyclic graph with maximum degree  $d$  and  $\nu$  v-structures. It is possible to identify all v-structures in  $O(\nu)$  estimates over subsets of at most size  $d + 2$ .*

*Proof.* Each v-structure  $i \rightarrow j \leftarrow k$  falls under two cases.

1.  $i \perp\!\!\!\perp k$  unconditionally. Then an estimate over  $\{i, j, k\}$  will identify the v-structure.
2.  $i \perp\!\!\!\perp k \mid S$ , where  $j \notin S \subset V$ . Then an estimate over  $S \cup \{i, j, k\}$  will identify the v-structure. Note that  $|S| \leq d + 2$  since the degree of  $i$  is at least  $|S| + 1$ .

Therefore, each v-structure only requires one estimate, and it is possible to identify all v-structures in  $O(\nu)$  estimates.  $\square$

There are three takeaways from this section.

1. If we exhaustively run a constraint-based algorithm on all subsets of size  $d + 2$ , it is trivial to recover the estimate of the full graph. However, this is no more efficient than running the causal discovery algorithm on the full graph.
2. In theory, it is possible to recover the undirected graph in  $O(N^2)$  estimates, and the v-structures in  $O(\nu)$  estimates. However, we may not know the appropriate subsets ahead of time.
3. In practice, if we have a surrogate for connectivity, such as the global statistics used in SEA, then we can vastly reduce the number of estimates used to eliminate edges from consideration, and more effectively focus on sampling subsets for orientation determination.

### A.3 Computational power of the axial attention model

Existing literature on the universality and computational power of vanilla Transformers (Yun et al., 2019; Pérez et al., 2019) rely on generous assumptions regarding depth or precision. Here, we show that our axial attention-based model can implement the specific reasoning required to resolve marginal estimates under realistic conditions. In particular, we show that three blocks can recover the skeleton and v-structures in  $O(N)$  width, and additional blocks have the capacity to propagate orientations. We first formalize the notion of a neural network architecture’s capacity to “implement” an algorithm. Then we prove Theorem 3.1 by construction.

**Definition A.11.** Let  $f$  be a map from finite sets  $Q$  to  $F$ , and let  $\phi$  be a map from finite sets  $Q_\Phi$  to  $F_\Phi$ . We say  $\phi$  implements  $f$  if there exists injection  $g_{\text{in}} : Q \rightarrow Q_\Phi$  and surjection  $g_{\text{out}} : F_\Phi \rightarrow F$  such that

$$\forall q \in Q, g_{\text{out}}(\phi(g_{\text{in}}(q))) = f(q). \quad (17)$$

**Definition A.12.** Let  $Q, F, Q_\Phi, F_\Phi$  be finite sets. Let  $f$  be a map from  $Q$  to  $F$ , and let  $\Phi$  be a finite set of maps  $\{\phi : Q_\Phi \rightarrow F_\Phi\}$ . We say  $\Phi$  has the capacity to implement  $f$  if and only if there exists at least one element  $\phi \in \Phi$  that implements  $f$ .

**Theorem 3.1.** Let  $G = (V, E)$  be a directed acyclic graph with maximum degree  $d$ . For  $S \subseteq V$ , let  $E'_S$  denote the marginal estimate over  $S$ . Let  $\mathcal{S}_d$  denote the superset that contains all subsets  $S \subseteq V$  of size at most  $d$ . Given  $\{E'_S\}_{S \in \mathcal{S}_d}$ , a stack of  $L$  axial attention blocks has the capacity to recover  $G$ 's skeleton and  $v$ -structures in  $O(N)$  width, and propagate orientations on paths of  $O(L)$  length.

*Proof.* We consider axial attention blocks with dot-product attention and omit layer normalization from our analysis, as is common in the Transformer universality literature Yun et al. (2019). Our inputs  $X \in \mathbb{R}^{d \times R \times C}$  consist of  $d$ -dimension embeddings over  $R$  rows and  $C$  columns. Since our axial attention only operates over one dimension at a time, we use  $X_{\cdot,c}$  to denote a 1D sequence of length  $R$ , given a fixed column  $c$ , and  $X_{r,\cdot}$  to denote a 1D sequence of length  $C$ , given a fixed row  $r$ . A single axial attention layer (with one head) consists of two attention layers and a feedforward network,

$$\text{Attn}_{\text{row}}(X_{\cdot,c}) = X_{\cdot,c} + W_O W_V X_{\cdot,c} \cdot \sigma \left[ (W_K X_{\cdot,c})^T W_Q X_{\cdot,c} \right], \quad (18)$$

$$X \leftarrow \text{Attn}_{\text{row}}(X)$$

$$\text{Attn}_{\text{col}}(X_{r,\cdot}) = X_{r,\cdot} + W_O W_V X_{r,\cdot} \cdot \sigma \left[ (W_K X_{r,\cdot})^T W_Q X_{r,\cdot} \right], \quad (19)$$

$$X \leftarrow \text{Attn}_{\text{col}}(X)$$

$$\text{FFN}(X) = X + W_2 \cdot \text{ReLU}(W_1 \cdot X + b_1 \mathbf{1}_L^T) + b_2 \mathbf{1}_L^T, \quad (20)$$

where  $W_O \in \mathbb{R}^{d \times d}$ ,  $W_V, W_K, W_Q \in \mathbb{R}^{d \times d}$ ,  $W_2 \in \mathbb{R}^{d \times m}$ ,  $W_1 \in \mathbb{R}^{m \times d}$ ,  $b_2 \in \mathbb{R}^d$ ,  $b_1 \in \mathbb{R}^m$ , and  $m$  is the hidden layer size of the feedforward network. For concision, we have omitted the  $r$  and  $c$  subscripts on the  $W$ s, but the row and column attentions use different parameters. Any row or column attention can take on the identity mapping by setting  $W_O, W_V, W_K, W_Q$  to  $d \times d$  matrices of zeros.

A single axial attention *block* consists of two axial attention layers  $\phi_E$  and  $\phi_\rho$ , connected via messages (Section 3.3)

$$\begin{aligned} h^{E,\ell} &= \phi_{E,\ell}(h^{E,\ell-1}) \\ h^{\rho,\ell-1} &\leftarrow W_{\rho,\ell} [h^{\rho,\ell-1}, m^{E \rightarrow \rho,\ell}] \\ h^{\rho,\ell} &= \phi_{\rho,\ell}(h^{\rho,\ell-1}) \\ h^{E,\ell} &\leftarrow h^{E,\ell} + m^{\rho \rightarrow E,\ell} \end{aligned}$$

where  $h^\ell$  denote the hidden representations of  $E$  and  $\rho$  at layer  $\ell$ , and the outputs of the axial attention block are  $h^{\rho,\ell}, h^{E,\ell}$ .

We construct a stack of  $L \geq 3$  axial attention blocks that implement Algorithm 1.

**Model inputs** Consider edge estimate  $E'_{i,j} \in \mathcal{E}$  in a graph of size  $N$ . Let  $e_i, e_j$  denote the endpoints of  $(i, j)$ . Outputs of the PC algorithm can be expressed by three endpoints:  $\{\emptyset, \bullet, \blacktriangleright\}$ . A directed edge from  $i \rightarrow j$  has endpoints  $(\bullet, \blacktriangleright)$ , the reversed edge  $i \leftarrow j$  has endpoints  $(\blacktriangleright, \bullet)$ , an undirected edge has endpoints  $(\bullet, \bullet)$ , and the lack of any edge between  $i, j$  has endpoints  $(\emptyset, \emptyset)$ .

Let  $\text{one-hot}_N(i)$  denote the  $N$ -dimensional one-hot column vector where element  $i$  is 1. We define the embedding of  $(i, j)$  as a  $d = 2N + 6$  dimensional vector,

$$g_{\text{in}}(E_{t,(i,j)}) = h_{(i,j)}^{E,0} = \begin{bmatrix} \text{one-hot}_3(e_i) \\ \text{one-hot}_3(e_j) \\ \text{one-hot}_N(i) \\ \text{one-hot}_N(j) \end{bmatrix}. \quad (21)$$

To recover graph structures from  $h^E$ , we simply read off the indices of non-zero entries ( $g_{\text{out}}$ ). We can set  $h^{\rho,0}$  to any  $\mathbb{R}^{d \times N \times N}$  matrix, as we do not consider its values in this analysis and discard it during the first step.

**Claim A.13.** (*Consistency*) The outputs of each step

1. are consistent with (21), and
2. are equivariant to the ordering of nodes in edges.

For example, if  $(i, j)$  is oriented as  $(\blacktriangleright, \bullet)$ , then we expect  $(j, i)$  to be oriented  $(\bullet, \blacktriangleright)$ .

**Step 1: Undirected skeleton** We use the first axial attention block to recover the undirected skeleton  $C'$ . We set all attentions to the identity, set  $W_{\rho,1} \in \mathbb{R}^{2d \times d}$  to a  $d \times d$  zeros matrix, stacked on top of a  $d \times d$  identity matrix (discard  $\rho$ ), and set  $\text{FFN}_E$  to the identity (inputs are positive). This yields

$$h_{i,j}^{\rho,0} = m_{i,j}^{E \rightarrow \rho,1} = \begin{bmatrix} P_{e_i}(\emptyset) \\ P_{e_i}(\bullet) \\ P_{e_i}(\blacktriangleright) \\ \vdots \\ \text{one-hot}_N(i) \\ \text{one-hot}_N(j) \end{bmatrix}, \quad (22)$$

where  $P_{e_i}(\cdot)$  is the frequency that endpoint  $e_i = \cdot$  within the subsets sampled. FFNs with 1 hidden layer are universal approximators of continuous functions (Hornik et al., 1989), so we use  $\text{FFN}_\rho$  to map

$$\text{FFN}_\rho(X_{i,u,v}) = \begin{cases} 0 & i \leq 6 \\ 0 & i > 6, X_{1,u,v} = 0 \\ -X_{i,u,v} & \text{otherwise,} \end{cases} \quad (23)$$

where  $i \in [2N + 6]$  indexes into the feature dimension, and  $u, v$  index into the rows and columns. This allows us to remove edges not present in  $C'$  from consideration:

$$m^{\rho \rightarrow E,1} = h^{\rho,1} \\ h_{i,j}^{E,1} \leftarrow h_{i,j}^{E,1} + m_{i,j}^{\rho \rightarrow E,1} = \begin{cases} 0 & (i,j) \notin C' \\ h_{i,j}^{E,0} & \text{otherwise.} \end{cases} \quad (24)$$

This yields  $(i,j) \in C'$  if and only if  $h_{i,j}^{\rho,1} \neq \mathbf{0}$ . We satisfy A.13 since our inputs are valid PC algorithm outputs for which  $P_{e_i}(\emptyset) = P_{e_j}(\emptyset)$ .

**Step 2: V-structures** The second and third axial attention blocks recover v-structures. We run the same procedure twice, once to capture v-structures that point towards the first node in an ordered pair, and one to capture v-structures that point towards the latter node.

We start with the first row attention over edge estimates, given a fixed subset  $t$ . We set the key and query attention matrices

$$W_K = k \cdot \begin{bmatrix} 0 & 0 & 1 & & & \\ & & & 0 & 1 & 0 \\ & \vdots & & & & \\ & & & & I_N & \\ & & & & & -I_N \end{bmatrix} \quad W_Q = k \cdot \begin{bmatrix} 0 & 0 & 1 & & & \\ & & & 0 & 1 & 0 \\ & \vdots & & & & \\ & & & & I_N & \\ & & & & & I_N \end{bmatrix} \quad (25)$$

where  $k$  is a large constant,  $I_N$  denotes the size  $N$  identity matrix, and all unmarked entries are 0s.

Recall that a v-structure is a pair of directed edges that share a target node. We claim that two edges  $(i,j), (u,v)$  form a v-structure in  $E'$ , pointing towards  $i = u$ , if this inner product takes on the maximum value

$$\langle (W_K h^{E,1})_{i,j}, (W_Q h^{E,1})_{u,v} \rangle = 3. \quad (26)$$

Suppose both edges  $(i,j)$  and  $(u,v)$  still remain in  $C'$ . There are two components to consider.

1. If  $i = u$ , then their shared node contributes +1 to the inner product (prior to scaling by  $k$ ). If  $j = v$ , then the inner product accrues  $-1$ .
2. Nodes that do not share the same endpoint contribute 0 to the inner product. Of edges that share one node, only endpoints that match  $\blacktriangleright$  at the starting node, or  $\bullet$  at the ending node contribute +1 to the inner product each. We provide some examples below.

$(e_i, e_j)$	$(e_u, e_v)$	contribution	note
$(\blacktriangleright, \bullet)$	$(\bullet, \blacktriangleright)$	0	no shared node
$(\bullet, \blacktriangleright)$	$(\bullet, \blacktriangleright)$	0	wrong endpoints
$(\bullet, \bullet)$	$(\bullet, \bullet)$	1	one correct endpoint
$(\blacktriangleright, \bullet)$	$(\blacktriangleright, \bullet)$	2	v-structure

All edges with endpoints  $\emptyset$  were “removed” in step 1, resulting in an inner product of zero, since their node embeddings were set to zero. We set  $k$  to some large constant (empirically,  $k^2 = 1000$  is more than enough) to ensure that after softmax scaling,  $\sigma_{e,e'} > 0$  only if  $e, e'$  form a v-structure.

Given ordered pair  $e = (i, j)$ , let  $V_i \subset V$  denote the set of nodes that form a v-structure with  $e$  with shared node  $i$ . Note that  $V_i$  excludes  $j$  itself, since setting of  $W_K, W_Q$  exclude edges that share both nodes. We set  $W_V$  to the identity, and we multiply by attention weights  $\sigma$  to obtain

$$(W_V h^{E,1} \sigma)_{e=(i,j)} = \left[ \frac{\begin{matrix} \vdots \\ \text{one-hot}_N(i) \end{matrix}}{\alpha_j \cdot \text{binary}_N(V_j)} \right] \quad (27)$$

where  $\text{binary}_N(S)$  denotes the  $N$ -dimensional binary vector with ones at elements in  $S$ , and the scaling factor

$$\alpha_j = (1/\|V_j\|) \cdot \mathbb{1}\{\|V_j\| > 0\} \in [0, 1] \quad (28)$$

results from softmax normalization. We set

$$W_O = \begin{bmatrix} \mathbf{0}_{N+6} & \\ & 0.5 \cdot I_N \end{bmatrix} \quad (29)$$

to preserve the original endpoint values, and to distinguish between the edge’s own node identity and newly recognized v-structures. To summarize, the output of this row attention layer is

$$\text{Attn}_{\text{row}}(X_{\cdot,c}) = X_{\cdot,c} + W_O W_V X_{\cdot,c} \cdot \sigma,$$

which is equal to its input  $h^{E,1}$  plus additional positive values  $\in (0, 0.5)$  in the last  $N$  positions that indicate the presence of v-structures that exist in the overall  $E'$ .

Our final step is to “copy” newly assigned edge directions into all the edges. We set the  $\phi_E$  column attention,  $\text{FFN}_E$  and the  $\phi_\rho$  attentions to the identity mapping. We also set  $W_{\rho,2}$  to a  $d \times d$  zeros matrix, stacked on top of a  $d \times d$  identity matrix. This passes the output of the  $\phi_E$  row attention, aggregated over subsets, directly to  $\text{FFN}_{\phi,2}$ .

For endpoint dimensions  $\mathbf{e} = [6]$ , we let  $\text{FFN}_{\phi,2}$  implement

$$\text{FFN}_{\rho,2}(X_{\mathbf{e},u,v}) = \begin{cases} [0, 0, 1, 0, 1, 0]^T - X_{\mathbf{e},u,v} & 0 < \sum_{i>N+6} X_{i,u,v} < 0.5 \\ 0 & \text{otherwise.} \end{cases} \quad (30)$$

Subtracting  $X_{\mathbf{e},u,v}$  “erases” the original endpoints and replaces them with  $(\blacktriangleright, \bullet)$  after the update

$$h_{i,j}^{E,1} \leftarrow h_{i,j}^{E,1} + m_{i,j}^{\rho \rightarrow E,1}.$$

The overall operation translates to checking whether *any* v-structure points towards  $i$ , and if so, assigning edge directions accordingly. For dimensions  $i > 6$ ,

$$\text{FFN}_{\rho,2}(X_{i,u,v}) = \begin{cases} -X_{i,u,v} & X_{i,u,v} \leq 0.5 \\ 0 & \text{otherwise,} \end{cases} \quad (31)$$

effectively erasing the stored v-structures from the representation and remaining consistent to (21).

At this point, we have copied all v-structures once. However, our orientations are not necessarily symmetric. For example, given v-structure  $i \rightarrow j \leftarrow k$ , our model orients edges  $(j, i)$  and  $(j, k)$ , but not  $(i, j)$  or  $(k, j)$ .

The simplest way to symmetrize these edges (for the writer and the reader) is to run another axial attention block, in which we focus on v-structures that point towards the second node of a pair. The only changes are as follows.

- For  $W_K$  and  $W_Q$ , we swap columns 1-3 with 4-6, and columns 7 to  $N + 6$  with the last  $N$  columns.
- $(h^{E,2} \sigma)_{i,j}$  sees the third and fourth blocks swapped.
- $W_O$  swaps the  $N \times N$  blocks that correspond to  $i$  and  $j$ ’s node embeddings.
- $\text{FFN}_{\rho,3}$  sets the endpoint embedding to  $[0, 1, 0, 0, 0, 1]^T - X_{\mathbf{e},u,v}$  if  $i = 7, \dots, N + 6$  sum to a value between 0 and 0.5.

The result is  $h^{E,3}$  with all v-structures oriented symmetrically, satisfying A.13.

**Step 3: Orientation propagation** To propagate orientations, we would like to identify cases  $(i, j), (i, k) \in E', (j, k) \notin E'$  with shared node  $i$  and corresponding endpoints  $(\blacktriangleright, \bullet), (\bullet, \bullet)$ . We use  $\phi_E$  to identify triangles, and  $\phi_\rho$  to identify edges  $(i, j), (i, k) \in E'$  with the desired endpoints, while ignoring triangles.

**Marginal layer** The row attention in  $\phi_E$  fixes a subset  $t$  and varies the edge  $(i, j)$ .

Given edge  $(i, j)$ , we want to extract all  $(i, k)$  that share node  $i$ . We set the key and query attention matrices to

$$W_K, W_Q = k \cdot \begin{bmatrix} 0 & 1 & 1 & 0 & 1 & 1 \\ \vdots & & & & & \\ & & & I_N & & \\ & & & & \pm I_N & \end{bmatrix}. \quad (32)$$

We set  $W_V$  to the identity to obtain

$$(W_V h^E \sigma)_{e=(i,k)} = \begin{bmatrix} \vdots \\ \vdots \\ \text{one-hot}_N(i) \\ \alpha_k \cdot \text{binary}_N(V_k) \end{bmatrix}, \quad (33)$$

where  $V_k$  is the set of nodes  $k$  that share any edge with  $i$ . To distinguish between  $k$  and  $V_k$ , we again set  $W_o$  to the same as in (29). Finally, we set  $\text{FFN}_E$  to the identity and pass  $h^E$  directly to  $\phi_\rho$ . To summarize, we have  $h^E$  equal to its input, with values  $\in (0, 0.5)$  in the last  $N$  locations indicating 1-hop neighbors of each edge.

**Global layer** Now we would like to identify cases  $(i, k), (j, k)$  with corresponding endpoints  $(\bullet, \blacktriangleright), (\bullet, \bullet)$ . We set the key and query attention matrices

$$W_K = k \cdot \begin{bmatrix} 0 & 0 & 1 \\ \vdots & & \\ & I_N & \\ & & I_N \end{bmatrix} \quad W_Q = k \cdot \begin{bmatrix} 0 & 1 & -1 & 0 & 1 & -1 \\ \vdots & & & & & \\ & & & I_N & & \\ & & & & -I_N & \end{bmatrix}. \quad (34)$$

The key allows us to check that endpoint  $i$  is directed, and the query allows us to check that  $(i, k)$  exists in  $C'$ , and does not already point elsewhere. After softmax normalization, for sufficiently large  $k$ , we obtain  $\sigma_{(i,j),(i,k)} > 0$  if and only if  $(i, k)$  should be oriented  $(\bullet, \blacktriangleright)$ , and the inner product attains the maximum possible value

$$\langle (W_K h^\rho)_{i,j}, (W_Q h^\rho)_{i,k} \rangle = 2. \quad (35)$$

We consider two components.

1. If the endpoints match our desired endpoints, we gain a +1 contribution to the inner product.
2. A match between the first nodes contributes +1. If the second node shares any overlap (either same edge, or a triangle), then a negative value would be added to the overall inner product.

Therefore, we can only attain the maximal inner product if only one edge is directed, and if there exists no triangle.

We set  $W_o$  to the same as in (29), and we add  $h^\rho$  to the input of the next  $\phi_E$ . To summarize, we have  $h^\rho$  equal to its input, with values  $\in (0, 0.5)$  in the last  $N$  locations indicating incoming edges.

**Orientation assignment** Our final step is to assign our new edge orientations. Let the column attention take on the identity mapping. For endpoint dimensions  $\mathbf{e} = (4, 5, 6)$ , we let  $\text{FFN}_\rho$  implement

$$\text{FFN}_\rho(X_{\mathbf{e},u,v}) = \begin{cases} [0, 0, 1]^T - X_{\mathbf{e},u,v} & 0 < \sum_{i>N+6} X_{i,u,v} < 0.5 \\ 0 & \text{otherwise.} \end{cases} \quad (36)$$

This translates to checking whether any incoming edge points towards  $v$ , and if so, assigning the new edge direction accordingly. For dimensions  $i > 6$ ,

$$\text{FFN}_\rho(X_{i,u,v}) = \begin{cases} 0 & X_{i,u,v} \leq 0.5 \\ X_{i,u,v} & \text{otherwise,} \end{cases} \quad (37)$$

effectively erasing the stored assignments from the representation. Thus, we are left with  $h^{E,\ell}$  that conforms to the same format as the initial embedding in (21).

To symmetrize these edges, we run another axial attention block, in which we focus on paths that point towards the second node of a pair. The only changes are as follows.

- For  $\phi_E$  layer  $W_K$  and  $W_Q$  (32), we swap  $I_N$  and  $\pm I_N$ .
- For  $\phi_\rho$  layer  $W_K$  and  $W_Q$  (34), we swap  $I_N$  and  $\pm I_N$ .
- $W_O$  swaps the  $N \times N$  blocks that correspond to  $i$  and  $j$ 's node embeddings.
- For  $\text{FFN}_\rho$  (36), we let  $\mathbf{e} = (1, 2, 3)$  instead.

The result is  $h^E$  with symmetric 1-hop orientation propagation, satisfying A.13. We may repeat this procedure  $k$  times to capture  $k$ -hop paths.

To summarize, we used axial attention block 1 to recover the undirected skeleton  $C'$ , blocks 2-3 to identify and copy v-structures in  $E'$ , and all subsequent  $L - 3$  layers to propagate orientations on paths up to  $\lfloor (L - 3)/2 \rfloor$  length. Overall, this particular construction requires  $O(N)$  width for  $O(L)$  paths.

□

**Final remarks** Information theoretically, it should be possible to encode the same information in  $\log N$  space, and achieve  $O(\log N)$  width. For ease of construction, we have allowed for wider networks than optimal.

On the other hand, if we increase the width and encode each edge symmetrically, e.g.  $(e_i, e_j, e_j, e_i \mid i, j, j, i)$ , we can reduce the number of blocks by half, since we no longer need to run each operation twice. However, attention weights scale quadratically, so we opted for an asymmetric construction.

Finally, a strict limitation of our model is that it only considers 1D pairwise interactions. In the graph layer, we cannot compare different edges' estimates at different times in a single step. In the feature layer, we cannot compare  $(i, j)$  to  $(j, i)$  in a single step either. However, the graph layer does enable us to compare all edges at once (sparsely), and the feature layer looks at a time-collapsed version of the whole graph. Therefore, though we opted for this design for computational efficiency, we have shown that it is able to capture significant graph reasoning.

#### A.4 Robustness and stability

We discuss the notion of stability informally, in the context of Spirtes et al. (2001). There are two cases in which our framework may receive erroneous inputs: low/noisy data settings, and functionally misspecified situations. We consider our framework's empirical robustness to these cases, in terms of recovering the skeleton and orienting edges.

In the case of noisy data, edges may be erroneously added, removed, or misdirected from marginal estimates  $E'$ . Our framework provides two avenues to mitigating such noise.

1. We observe that global statistics can be estimated reliably in low data scenarios. For example, Figure 5 suggests that 200 examples suffice to provide a robust estimate over 100 variables in our synthetic settings. Therefore, even if the marginal estimates are erroneous, the neural network can learn the skeleton from the global statistics.
2. Most classical causal discovery algorithms are not stable with respect to edge orientation assignment. That is, an error in a single edge may propagate throughout the graph. Empirically, we observe that the majority vote of GIES achieves reasonable accuracy even without any training, while FCI suffers in this assessment (Table ??). However both SEA (GIES)

and SEA (FCI) achieve high edge accuracy. Therefore, while the underlying algorithms may not be stable with respect to edge orientation, our pretrained aggregator seems to be robust.

It is also possible that our global statistics and marginal estimates make misspecified assumptions regarding the data generating mechanisms. The degree of misspecification can vary case by case, so it is hard to provide any broad guarantees about the performance of our algorithm, in general. However, we can make the following observation.

If two variables are independent,  $X_i \perp\!\!\!\perp X_j$ , they are independent, e.g. under linear Gaussian assumptions. If  $X_i, X_j$  exhibit more complex functional dependencies, they may be erroneously deemed independent. Therefore, any systematic errors are necessarily one-sided, and the model can learn to recover the connectivity based on global statistics.

## B Experimental details

### B.1 Synthetic data generation

Synthetic datasets were generated using code from DCDI (Brouillard et al., 2020), which extended the Causal Discovery Toolkit data generators to interventional data (Kalainathan et al., 2020).

We considered the following causal mechanisms. Let  $y$  be the node in question, let  $X$  be its parents, let  $E$  be an independent noise variable (details below), and let  $W$  be randomly initialized weight matrices.

- Linear:  $y = XW + E$ .
- Polynomial:  $y = W_0 + XW_1 + X^2W_2 + \dots + E$
- Sigmoid:  $y = \sum_{i=1}^d W_i \cdot \text{sigmoid}(X_i) + \dots + E$
- Randomly initialized neural network (NN):  $y = \text{Tanh}((X, E)W_{\text{in}})W_{\text{out}}$
- Randomly initialized neural network, additive (NN additive):  $y = \text{Tanh}(XW_{\text{in}})W_{\text{out}} + E$

Root causal mechanisms, noise variables, and interventional distributions maintained the DCDI defaults.

- Root causal mechanisms were set to  $\text{Uniform}(-2, 2)$ .
- Noise was set to  $E \sim 0.4 \cdot \mathcal{N}(0, \sigma^2)$  where  $\sigma^2 \sim \text{Uniform}(1, 2)$ .
- Interventions were applied to all nodes (one at a time) by setting their causal mechanisms to  $\mathcal{N}(0, 1)$ .

Ablation datasets with  $N > 100$  nodes contained 100,000 points each (same as  $N = 100$ ). We set random seeds for each dataset using the hash of the output filename.

### B.2 Baseline details

We considered the following baselines. All baselines were run using official implementations published by the authors.

**DCDI** (Brouillard et al., 2020) was trained on each of the  $N = 10, 20$  datasets using their published hyperparameters. We denote the Gaussian and Deep Sigmoidal Flow versions as DCDI-G and DCDI-DSF respectively. DCDI could not scale to graphs with  $N = 100$  due to memory constraints (did not fit on a 32GB V100 GPU).

**DCD-FG** (Lopez et al., 2022) was trained on all of the test datasets using their published hyperparameters. We set the number of factors to 5, 10, 20 for each of  $N = 10, 20, 100$ , based on their ablation studies. Due to numerical instability on  $N = 100$ , we clamped augmented Lagrangian multipliers  $\mu$  and  $\gamma$  to 10 and stopped training if elements of the learned adjacency matrix reached NaN values. After discussion with the authors, we also tried adjusting the  $\mu$  multiplier from 2 to 1.1, but the model did not converge within 48 hours.

**DECI** (Geffner et al., 2022) was trained on all of the test datasets using their published hyperparameters. However, on all  $N = 100$  cases, the model failed to produce any meaningful results (adjacency matrices nearly all remained 0s with AUCs of 0.5). Thus, we only report results on  $N = 10, 20$ .

**DIFFAN** (Sanchez et al., 2023) was trained on each of the  $N = 10, 20$  datasets using their published hyperparameters. The authors write that “most hyperparameters are hard-coded into [the] constructor of the DIFFAN class and we verified they work across a wide set of datasets.” We used the original, non-approximation version of their algorithm by maintaining `residue=True` in their codebase. We were unable to consistently run DIFFAN with both R and GPU support within a Docker container, and the authors did not respond to questions regarding reproducibility, so all models were trained on the CPU only. We observed approximately a 10x speedup in the  $< 5$  cases that were able to complete running on the GPU.

**AVICI** (Lorch et al., 2022) was run on all test datasets using the authors’ pretrained `scm-v0` model, recommended for “arbitrary real-valued data.” Note that this model is different from the models described in their paper (denoted AVICI-L and AVICI-R), as it was trained on *all* of their synthetic data, including test sets. We sampled 1000 observations per dataset uniformly at random, with their respective interventions (the maximum number of synthetic samples used in their original paper), except for Sachs, which used the entire dataset (as in their paper). Though the authors provided separate weights for synthetic mRNA data, we were unable to use it since we did not preserve the raw gene counts in our simulated mRNA datasets.

**INVCOV** computes inverse covariance over 1000 examples. This does *not* orient edges, but it is a strong connectivity baseline. We discretize based on ground truth positive rate.

**CORR** and **D-CORR** are computed similarly, using global correlation and distance correlation, respectively (See C.2 for details).

### B.3 Neural network design

Hyperparameters and architectural choices were selected by training the model on 20% of the training and validation data for approximately 50k steps (several hours). We considered the following parameters in sequence.

- learned positional embedding vs. sinusoidal positional embedding
- number of layers  $\times$  number of heads:  $\{4, 8\} \times \{4, 8\}$
- learning rate  $\eta = \{1e - 4, 5e - 5, 1e - 5\}$

For our final model, we selected learned positional embeddings, 4 layers, 8 heads, and learning rate  $\eta = 1e - 4$ .

### B.4 Training and hardware details

The models were trained across 2 NVIDIA RTX A6000 GPUs and 60 CPU cores. We used the GPU exclusively for running the aggregator, and retained all classical algorithm execution on the CPUs (during data loading). The total pretraining time took approximately 14 hours for the final FCI model and 16 hours for the final GIES model.

For finetuning, we used rank  $r = 2$  adapters on the axial attention model’s key, query, and feedforward weights (Hu et al., 2022). We trained until convergence on the validation set (no improvement for 100 epochs), which took 4-6 hours with 40 CPUs and around 10 hours with 20 CPUs. We used a single NVIDIA RTX A6000 GPU, but the bottleneck was CPU availability.

For the scope of this paper, our models and datasets are fairly small. We did not scale further due to hardware constraints. Our primary bottlenecks to scaling up lay in availability of CPU cores and networking speed across nodes, rather than GPU memory or utilization. The optimal CPU:GPU ratio for SEA ranges from 20:1 to 40:1.

We are able to run inference comfortably over  $N = 500$  graphs with  $T = 500$  subsets of  $k = 5$  nodes each, on a single 32GB V100 GPU. For runtime analysis, we used a batch size of 1, with 1 data worker per dataset. Our runtime could be further improved if we amortized the GPU utilization across batches.

## B.5 Choice of classical causal discovery algorithm

For training, we selected FCI (Spirtes et al., 1995) as the underlying discovery algorithm in the observational setting over GES (Chickering, 2002), GRaSP (Lam et al., 2022), and LiNGAM (Shimizu et al., 2006) due to its speed and superior downstream performance. We hypothesize this may be due to its richer output (ancestral graph) providing more signal to the Transformer model. We also tried Causal Additive Models (Bühlmann et al., 2014), but its runtime was too slow for consistent GPU utilization. Observational algorithm implementations were provided by the causal-learn library (Zheng et al., 2023). The code for running these alternative classical algorithms is available in our codebase.

We selected GIES as the discovery algorithm in the interventional setting because an efficient Python implementation was readily available at <https://github.com/juangame11a/gies>.

We tried incorporating implementations from the Causal Discovery Toolbox via a Docker image (Kalainathan et al., 2020), but there was excessive overhead associated with calling an R subroutine and reading/writing the inputs/results from disk.

Finally, we considered other independence tests for richer characterization, such as kernel-based methods. However, due to speed, we chose to remain with the default Fisherz conditional independence test for FCI, and BIC for GIES (Schwarz, 1978).

## B.6 Sampling procedure

**Selection scores:** We consider three strategies for computing selection scores  $\alpha$ . We include an empirical comparison of these strategies in Table 6.

1. Random selection:  $\alpha$  is an  $N \times N$  matrix of ones.
2. Global-statistic-based selection:  $\alpha = \rho$ .
3. Uncertainty-based selection:  $\alpha = \hat{H}(E_t)$ , where  $H$  denotes the information entropy

$$\alpha_{i,j} = - \sum_{e \in \{0,1,2\}} p(e) \log p(e). \quad (38)$$

Let  $c_{i,j}^t$  be the number of times edge  $(i,j)$  was selected in  $S_1 \dots S_{t-1}$ , and let  $\alpha^t = \alpha / \sqrt{c_{i,j}^t}$ . We consider two strategies for selecting  $S_t$  based on  $\alpha_t$ .

**Greedy selection:** Throughout our experiments, we used a greedy algorithm for subset selection. We normalize probabilities to 1 before the constructing each Categorical. Initialize

$$S_t \leftarrow \{i : i \sim \text{Categorical}(\alpha_1^t \dots \alpha_N^t)\}. \quad (39)$$

where  $\alpha_i^t = \sum_{j \neq i \in V} \alpha_{i,j}^t$ . While  $|S_t| < k$ , update

$$S_t \leftarrow S_t \cup \{j : j \sim \text{Categorical}(\alpha_{1,S_t}^t \dots \alpha_{N,S_t}^t)\} \quad (40)$$

where

$$\alpha_{j,S_t} = \begin{cases} \sum_{i \in S_t} \alpha_{i,j}^t & j \notin S_t \\ 0 & \text{otherwise.} \end{cases} \quad (41)$$

**Subset selection:** We also considered the following subset-level selection procedure, and observed minor performance gain for significantly longer runtime (linear program takes around 1 second per batch). Therefore, we opted for the greedy method instead.

We solve the following integer linear program to select a subset  $S_t$  of size  $k$  that maximizes  $\sum_{i \in S_t} \alpha_{i,j}^t$ . Let  $\nu_i \in \{0,1\}$  denote the selection of node  $i$ , and let  $\epsilon_{i,j} \in \{0,1\}$  denote the selection of edge  $(i,j)$ . Our objective is to

$$\begin{aligned} & \text{maximize} && \sum_{i,j} \alpha_{i,j}^t \cdot \epsilon_{i,j} \\ & \text{subject to} && \sum_i \nu_i = k && \text{subset size} \\ & && \epsilon_{i,j} \geq \nu_i + \nu_j - 1 && \text{node-edge consistency} \\ & && \epsilon_{i,j} \leq \nu_i \\ & && \epsilon_{i,j} \leq \nu_j, \\ & && \nu_i \in \{0,1\} \\ & && \epsilon_{i,j} \in \{0,1\} \end{aligned}$$

Table 6: Comparison between heuristics-based sampler (random and inverse covariance) vs. model confidence-based sampler. The suffix -L indicates the greedy confidence-based sampler. Each setting encompasses 5 distinct Erdős-Rényi graphs. The symbol † indicates that SEA was not pretrained on this setting. Bold indicates best of all models considered (including baselines not pictured).

$N$	$E$	Model	Linear			NN add.			NN non-add.			Sigmoid†			Polynomial†		
			mAP↑	OA↑	shd↓	mAP↑	OA↑	shd↓	mAP↑	OA↑	shd↓	mAP↑	OA↑	shd↓	mAP↑	OA↑	shd↓
10	10	SEA-F	0.97	0.92	1.6	<b>0.95</b>	<b>0.92</b>	2.4	<b>0.92</b>	0.94	2.8	0.83	0.76	3.7	0.69	0.71	6.7
		SEA-G	<b>0.99</b>	<b>0.94</b>	1.2	0.94	0.88	2.6	0.91	0.93	3.2	0.85	0.84	4.0	0.70	0.79	<b>5.8</b>
		SEA-F-L	0.97	0.93	<b>1.0</b>	0.95	0.87	2.4	<b>0.92</b>	<b>0.98</b>	3.4	0.84	0.77	3.9	<b>0.70</b>	0.79	<b>5.8</b>
		SEA-G-L	0.98	0.93	1.4	0.94	0.91	2.8	0.91	0.94	4.0	<b>0.88</b>	<b>0.84</b>	<b>3.6</b>	0.70	<b>0.80</b>	<b>5.8</b>
10	40	SEA-F	0.90	0.87	14.4	0.91	0.94	11.2	0.87	0.86	16.0	<b>0.81</b>	0.85	22.7	0.81	0.92	33.4
		SEA-G	<b>0.94</b>	<b>0.91</b>	<b>12.8</b>	0.91	<b>0.95</b>	<b>10.4</b>	<b>0.89</b>	<b>0.89</b>	17.2	0.81	<b>0.87</b>	24.5	0.89	0.93	29.5
		SEA-F-L	0.91	0.90	15.6	<b>0.91</b>	0.92	15.8	0.88	0.86	14.2	0.81	0.84	23.2	0.82	0.93	33.8
		SEA-G-L	0.93	0.91	13.4	0.91	0.93	<b>10.4</b>	0.88	0.85	16.2	0.79	0.83	25.5	<b>0.90</b>	<b>0.94</b>	28.3
20	20	SEA-F	0.97	0.92	3.2	0.94	0.97	3.2	0.84	0.93	7.2	0.84	0.85	7.6	<b>0.71</b>	<b>0.80</b>	10.2
		SEA-G	0.97	0.89	3.0	<b>0.94</b>	0.95	3.4	0.83	0.94	7.8	0.84	0.83	8.1	0.69	0.78	10.1
		SEA-F-L	0.97	<b>0.92</b>	2.8	0.93	0.95	3.8	<b>0.85</b>	0.94	6.8	<b>0.85</b>	0.85	<b>7.5</b>	0.67	0.78	<b>9.9</b>
		SEA-G-L	<b>0.97</b>	0.90	<b>2.6</b>	<b>0.94</b>	<b>0.98</b>	3.4	0.83	<b>0.97</b>	7.0	0.84	0.84	7.9	0.67	0.79	10.6
20	80	SEA-F	0.86	<b>0.93</b>	29.6	0.55	0.90	73.6	0.72	<b>0.93</b>	51.8	<b>0.77</b>	0.85	42.8	0.61	0.89	61.8
		SEA-G	<b>0.89</b>	0.92	<b>26.8</b>	<b>0.58</b>	0.88	71.4	0.73	0.92	50.6	0.76	0.84	45.0	<b>0.65</b>	<b>0.89</b>	60.1
		SEA-F-L	0.86	0.92	32.0	0.55	<b>0.90</b>	74.0	0.74	0.93	49.2	0.76	<b>0.87</b>	<b>41.8</b>	0.59	0.88	62.3
		SEA-G-L	<b>0.89</b>	0.92	28.4	0.58	0.89	71.6	0.75	0.92	49.4	0.75	0.85	45.7	<b>0.65</b>	0.88	60.6

for  $i, j \in V \times V, i \in V$ .  $S_t$  is the set of non-zero indices in  $\nu$ .

The final algorithm used the greedy selection strategy, with the first half of batches sampled according to global statistics, and the latter half sampled randomly, with visit counts shared. This strategy was selected heuristically, and we did not observe significant improvements or drops in performance when switching to other strategies (e.g. all greedy statistics-based, greedy uncertainty-based, linear program uncertainty-based, etc.)

Table 6 compares the heuristics-based greedy sampler (inverse covariance + random) with the model uncertainty-based greedy sampler. Runtimes are plotted in Figure 4. The latter was run on CPU only, since it was non-trivial to access the GPU within a PyTorch data loader. We ran a forward pass to obtain an updated selection score every 10 batches, so this accrued over 10 times the number of forward passes, all on CPU. With proper engineering, this model-based sampler is expected to be much more efficient than reported. Still, it is faster than nearly all baselines.

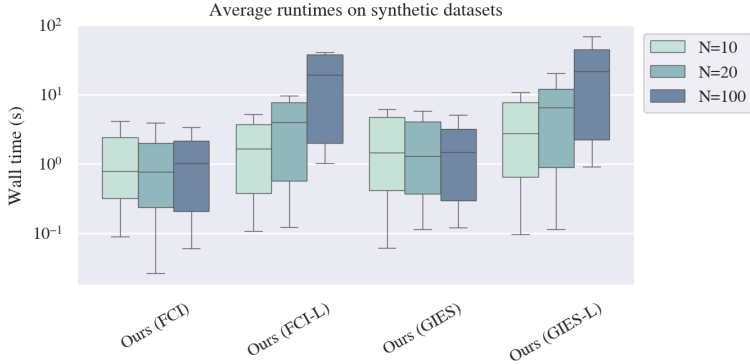


Figure 4: Runtime for heuristics-based greedy sampler vs. model uncertainty-based greedy sampler (suffix -L). For sampling, the model was run on CPU only, due to the difficulty of invoking GPU in the PyTorch data sampler.

## C Additional analyses

### C.1 Traditional algorithm parameters

We investigated model performance with respect to the settings of our graph estimation parameters. Our model is sensitive to the size of batches used to estimate global features and marginal graphs (Figure 5). In particular, at least 250 points are required per batch for an acceptable level of performance. Our model is not particularly sensitive to the number of batches sampled (Figure 6), or to the number of variables in each subset (Figure 7).

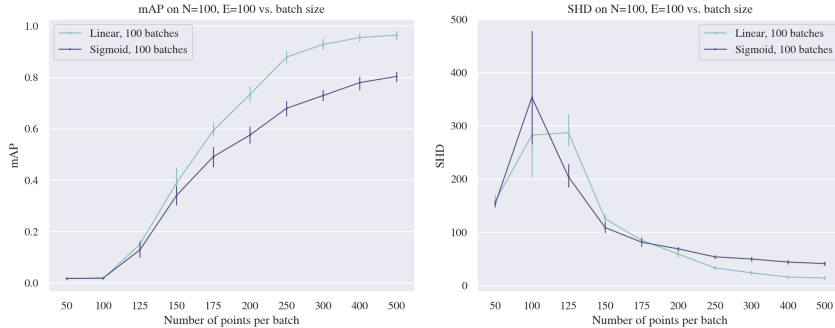


Figure 5: Performance of our model (GIES) as a function of traditional algorithm batch size. Error bars indicate 95% confidence interval across the 10 datasets of each setting. The global feature and marginal graph estimates are sensitive to batch size and require at least 250 points per batch to achieve an acceptable level of performance.

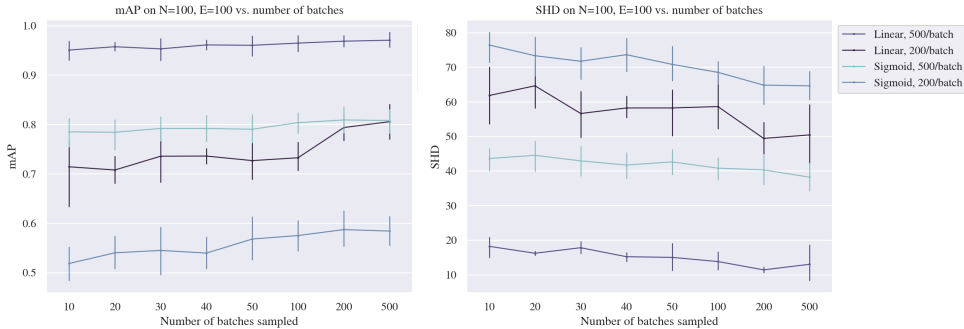


Figure 6: Performance of our model (GIES) as a function of number of batches sampled. Error bars indicate 95% confidence interval across the 10 datasets of each setting. Our model is relatively insensitive to the number of batches sampled, though more batches are beneficial in harder cases, e.g. sigmoid mechanism with additive noise or smaller batch size.

### C.2 Choice of global statistic

We selected inverse covariance as our global feature due to its ease of computation and its relationship to partial correlation. For context, we also provide the performance analysis of several alternatives. Tables 7 and 8 compare the results of different graph-level statistics on our synthetic datasets. Discretization thresholds for SHD were obtained by computing the  $p^{\text{th}}$  quantile of the computed values, where  $p = 1 - (E/N)$ . This is not entirely fair, as no other baseline receives the same calibration, but these ablation studies only seek to compare state-of-the-art causal discovery methods with the “best” possible (oracle) statistical alternatives.

**CORR** refers to global correlation,

$$\rho_{i,j} = \frac{\mathbb{E}(X_i X_j) - \mathbb{E}(X_i) \mathbb{E}(X_j)}{\sqrt{\mathbb{E}(X_i^2) - \mathbb{E}(X_i)^2} \cdot \sqrt{\mathbb{E}(X_j^2) - \mathbb{E}(X_j)^2}}. \quad (42)$$

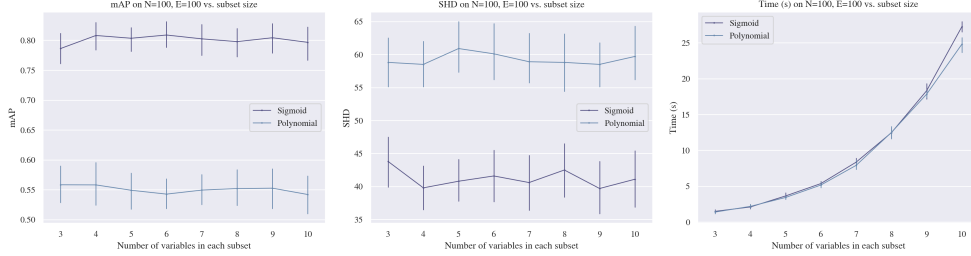


Figure 7: Performance of our model (GIES) as a function of subset size  $|S|$  (number of variables sampled). Error bars indicate 95% confidence interval across the 10 datasets of each setting. Our model was trained on  $|S| = 5$ , but it is insensitive to the number of variables sampled per subset at inference. Runtime scales exponentially upwards.

**D-CORR** refers to distance correlation, computed between all pairs of variables. Distance correlation captures both linear and non-linear dependencies, and  $\text{D-CORR}(X_i, X_j) = 0$  if and only if  $X_i \perp\!\!\!\perp X_j$ . Please refer to Sz'ekely et al. (2007) for the full derivation. Despite its power to capture non-linear dependencies, we opted not to use D-CORR because it is quite slow to compute between all pairs of variables.

**INVCOV** refers to inverse covariance, computed globally,

$$\rho = \mathbb{E}((X - \mathbb{E}(X))(X - \mathbb{E}(X))^T)^{-1}. \quad (43)$$

For graphs  $N < 100$ , inverse covariance was computed directly using NumPy. For graphs  $N \geq 100$ , inverse covariance was computed using Ledoit-Wolf shrinkage at inference time Ledoit & Wolf (2004). Unfortunately we only realized this after training our models, so swapping to Ledoit-Wolf leads to some distribution shift (and drop in performance) on SEA results for large graphs.

Table 7: Comparison of global statistics (continuous metrics). All standard deviations within 0.1.

$N$	$E$	Model	Linear		NN add.		NN non-add.		Sigmoid		Polynomial	
			mAP $\uparrow$	AUC $\uparrow$								
10	10	CORR	0.45	0.87	0.41	0.86	0.41	0.85	0.46	0.86	0.45	0.85
		D-CORR	0.42	0.86	0.41	0.87	0.40	0.87	0.43	0.86	0.45	0.89
		INVCOV	0.49	0.87	0.45	0.86	0.36	0.81	0.44	0.86	0.45	0.83
10	40	CORR	0.47	0.53	0.47	0.52	0.46	0.52	0.48	0.53	0.48	0.54
		D-CORR	0.46	0.53	0.46	0.51	0.46	0.54	0.48	0.53	0.47	0.54
		INVCOV	0.50	0.57	0.48	0.52	0.47	0.53	0.47	0.50	0.48	0.52
100	100	CORR	0.42	0.99	0.25	0.94	0.25	0.93	0.42	0.98	0.35	0.91
		D-CORR	0.41	0.99	0.25	0.96	0.26	0.96	0.41	0.98	0.37	0.94
		INVCOV	0.40	0.99	0.22	0.94	0.16	0.87	0.40	0.97	0.36	0.90
100	400	CORR	0.19	0.80	0.10	0.63	0.14	0.72	0.27	0.84	0.20	0.72
		D-CORR	0.19	0.80	0.10	0.63	0.14	0.75	0.26	0.84	0.21	0.74
		INVCOV	0.25	0.91	0.09	0.62	0.14	0.77	0.27	0.86	0.20	0.67

### C.3 Results on simulated mRNA data

We generated mRNA data using the SERGIO simulator Dibaeinia & Sinha (2020). We sampled datasets with the Hill coefficient set to  $\{0.25, 0.5, 1, 2, 4\}$  for training, and 2 for testing (2 was default). We set the decay rate to the default 0.8, and the noise parameter to the default of 1.0. We sampled 400 graphs for each of  $N = \{10, 20\}$  and  $E = \{N, 2N\}$ .

These data distributions are quite different from typical synthetic datasets, as they simulate steady-state measurements and the data are lower bounded at 0 (gene counts). Thus, we trained a separate model on these data using the SEA (FCI) architecture. Table 9 shows that SEA performs best across the board.

Table 8: Comparison of global statistics (SHD). Discretization thresholds for SHD were obtained by computing the  $p^{\text{th}}$  quantile of the computed values, where  $p = 1 - (E/N)$ .

$N$	$E$	Model	Linear	NN add.	NN non-add.	Sigmoid	Polynomial
10	10	CORR	10.6±2.8	10.2±4.6	12.0±1.9	11.1±4.3	9.9±2.8
		D-CORR	10.4±2.6	9.8±4.7	12.2±2.6	10.8±3.3	10.2±3.2
		INVCOV	11.0±2.8	11.4±5.5	13.6±2.9	11.4±4.1	10.9±3.5
10	40	CORR	39.2±2.4	38.0±1.8	38.2±0.7	38.8±3.3	38.2±2.0
		D-CORR	38.8±2.0	38.8±1.5	37.0±0.6	38.9±3.2	38.0±2.0
		INVCOV	35.8±2.3	39.2±1.5	37.6±2.7	40.7±2.2	38.4±1.2
100	100	CORR	113.0±4.9	132.2±18.0	144.6±5.2	106.5±11.5	110.3±6.1
		D-CORR	113.8±5.3	133.2±17.9	144.2±6.7	108.5±11.9	109.5±5.7
		INVCOV	124.4±8.1	130.0±17.2	158.8±6.2	112.3±14.8	106.3±4.6
100	400	CORR	580.4±24.5	666.0±13.5	626.2±23.4	516.5±18.5	562.5±20.1
		D-CORR	578.2±24.7	665.4±15.4	626.6±21.9	522.3±17.6	557.2±20.4
		INVCOV	557.0±11.7	667.8±15.4	639.0±9.7	514.7±23.1	539.4±18.4

Table 9: Causal discovery results on simulated mRNA data. Each setting encompasses 5 distinct scale-free graphs. Data were generated via SERGIO Dibacina & Sinha (2020).

$N$	$E$	Model	mAP ↑	AUC ↑	SHD ↓	OA ↑
10	10	DCDI-G	0.48±0.1	0.73±0.1	16.1±3.3	0.59±0.2
		DCDI-DSF	0.63±0.1	0.84±0.1	18.5±2.7	0.79±0.2
		DCD-FG	0.59±0.2	0.82±0.1	81.0±0.0	0.79±0.2
		AVICI	0.58±0.2	0.85±0.1	6.4±4.7	0.72±0.2
		SEA (FCI)	<b>0.92±0.1</b>	<b>0.98±0.0</b>	<b>1.9±2.0</b>	<b>0.92±0.1</b>
10	20	DCDI-G	0.32±0.1	0.57±0.1	26.2±1.3	0.47±0.2
		DCDI-DSF	0.44±0.1	0.64±0.1	25.7±1.3	0.63±0.1
		DCD-FG	0.43±0.1	0.69±0.1	73.0±0.0	0.67±0.2
		AVICI	0.22±0.1	0.44±0.2	16.8±1.5	0.27±0.3
		SEA (FCI)	<b>0.76±0.1</b>	<b>0.90±0.1</b>	<b>8.8±1.5</b>	<b>0.85±0.1</b>
20	20	DCDI-G	0.48±0.1	0.86±0.1	37.3±2.8	0.65±0.1
		DCDI-DSF	0.45±0.1	0.92±0.0	51.9±15.8	0.81±0.1
		DCD-FG	0.34±0.2	0.87±0.0	361±0	0.66±0.2
		AVICI	0.32±0.2	0.78±0.1	18.7±4.9	0.66±0.2
		SEA (FCI)	<b>0.54±0.2</b>	<b>0.94±0.0</b>	<b>16.6±3.3</b>	<b>0.83±0.1</b>
20	40	DCDI-G	0.31±0.1	0.65±0.1	54.7±2.7	0.49±0.1
		DCDI-DSF	0.40±0.1	0.71±0.1	54.6±4.4	0.63±0.1
		DCD-FG	0.36±0.1	0.77±0.1	343±0	0.67±0.1
		AVICI	0.17±0.1	0.54±0.1	37.1±1.9	0.46±0.1
		SEA (FCI)	<b>0.50±0.1</b>	<b>0.85±0.1</b>	<b>31.4±4.9</b>	<b>0.78±0.1</b>

#### C.4 Results and ablation studies on synthetic data

For completeness, we include additional results and analysis on the synthetic datasets. Tables 13 and 14 compare all baselines across all metrics and graph sizes on Erdős-Rényi graphs. Tables 15 and 16 include the same evaluation on scale-free graphs. Tables 17 and 18 assess  $N = 100$  graphs.

Table 11 ablates the contribution of the global and marginal features by setting their hidden representations to zero. Note that our model has never seen this type of input during training, so drops in performance may be conflated with input distributional shift. Overall, removing the joint statistics ( $h^p \leftarrow 0$ ) leads to a higher performance drop than removing the marginal estimates ( $h^E \leftarrow 0$ ). However, the gap between these ablation studies and our final performance may be quite large in some cases, so both inputs are important to the prediction.

Table 10: Scaling to synthetic graphs, larger than those seen in training. Each setting encompasses 5 distinct Erdős-Rényi graphs. All SEA runs in this table used  $T = 500$  subsets of nodes, with  $b = 500$  examples per batch. For AVICI, we took  $M = 2000$  samples per dataset (higher than maximum analyzed in their paper), since it performed better than  $M = 1000$ . Here, the mean AUC values are artificially high due to the high negative rates, as actual edges scale linearly as  $N$ , while the number of possible edges scales quadratically.

$N$	Model	Linear, $E = N$				Linear, $E = 4N$			
		mAP $\uparrow$	AUC $\uparrow$	SHD $\downarrow$	OA $\uparrow$	mAP $\uparrow$	AUC $\uparrow$	SHD $\downarrow$	OA $\uparrow$
100	INVCOV	0.43 $\pm$ 0.0	0.99 $\pm$ 0.0	117 $\pm$ 7	—	0.30 $\pm$ 0.0	0.93 $\pm$ 0.0	512 $\pm$ 11	—
	CORR	0.42 $\pm$ 0.0	0.99 $\pm$ 0.0	113 $\pm$ 5	—	0.19 $\pm$ 0.0	0.80 $\pm$ 0.0	579 $\pm$ 25	—
	AVICI	0.03 $\pm$ 0.0	0.43 $\pm$ 0.1	109 $\pm$ 6	0.49 $\pm$ 0.0	0.11 $\pm$ 0.0	0.55 $\pm$ 0.1	394 $\pm$ 14	0.58 $\pm$ 0.0
	SEA (FCI)	<b>0.97</b> $\pm$ 0.0	<b>1.00</b> $\pm$ 0.0	<b>11.6</b> $\pm$ 4.3	<b>0.93</b> $\pm$ 0.0	0.88 $\pm$ 0.0	0.98 $\pm$ 0.0	129 $\pm$ 10	0.94 $\pm$ 0.0
	SEA (GIES)	<b>0.97</b> $\pm$ 0.0	<b>1.00</b> $\pm$ 0.0	12.8 $\pm$ 4.7	0.91 $\pm$ 0.0	<b>0.91</b> $\pm$ 0.0	<b>0.99</b> $\pm$ 0.0	<b>105</b> $\pm$ 6	<b>0.95</b> $\pm$ 0.0
	200	INVCOV	0.45 $\pm$ 0.0	1.00 $\pm$ 0.0	218 $\pm$ 11	—	0.33 $\pm$ 0.0	0.96 $\pm$ 0.0	1000 $\pm$ 23
CORR		0.42 $\pm$ 0.0	0.99 $\pm$ 0.0	223 $\pm$ 8	—	0.18 $\pm$ 0.0	0.86 $\pm$ 0.0	1184 $\pm$ 25	—
AVICI		0.00 $\pm$ 0.0	0.36 $\pm$ 0.1	207 $\pm$ 10	0.41 $\pm$ 0.1	0.05 $\pm$ 0.0	0.53 $\pm$ 0.1	827 $\pm$ 37	0.54 $\pm$ 0.1
SEA (FCI)		0.91 $\pm$ 0.0	<b>1.00</b> $\pm$ 0.0	49.9 $\pm$ 5.4	0.87 $\pm$ 0.0	0.82 $\pm$ 0.0	0.97 $\pm$ 0.0	327 $\pm$ 52	0.92 $\pm$ 0.0
SEA (GIES)		<b>0.95</b> $\pm$ 0.0	<b>1.00</b> $\pm$ 0.0	<b>35.4</b> $\pm$ 5.7	<b>0.91</b> $\pm$ 0.0	<b>0.86</b> $\pm$ 0.0	<b>0.98</b> $\pm$ 0.0	<b>272</b> $\pm$ 50	<b>0.92</b> $\pm$ 0.0
300		INVCOV	0.46 $\pm$ 0.0	<b>1.00</b> $\pm$ 0.0	308 $\pm$ 20	—	0.35 $\pm$ 0.0	0.98 $\pm$ 0.0	1445 $\pm$ 56
	CORR	0.42 $\pm$ 0.0	1.00 $\pm$ 0.0	326 $\pm$ 21	—	0.20 $\pm$ 0.0	0.89 $\pm$ 0.0	1710 $\pm$ 82	—
	AVICI	0.01 $\pm$ 0.0	0.70 $\pm$ 0.0	298 $\pm$ 19	0.64 $\pm$ 0.0	0.02 $\pm$ 0.0	0.50 $\pm$ 0.0	1214 $\pm$ 68	0.51 $\pm$ 0.0
	SEA (FCI)	0.80 $\pm$ 0.0	1.00 $\pm$ 0.0	121 $\pm$ 14	0.78 $\pm$ 0.0	0.70 $\pm$ 0.0	0.95 $\pm$ 0.0	693 $\pm$ 67	0.86 $\pm$ 0.0
	SEA (GIES)	<b>0.88</b> $\pm$ 0.0	<b>1.00</b> $\pm$ 0.0	<b>88.9</b> $\pm$ 11.3	<b>0.84</b> $\pm$ 0.0	<b>0.78</b> $\pm$ 0.0	<b>0.96</b> $\pm$ 0.0	<b>556</b> $\pm$ 71	<b>0.87</b> $\pm$ 0.0
	400	INVCOV	0.47 $\pm$ 0.0	1.00 $\pm$ 0.0	418 $\pm$ 7	—	0.36 $\pm$ 0.0	0.98 $\pm$ 0.0	1883 $\pm$ 28
CORR		0.42 $\pm$ 0.0	1.00 $\pm$ 0.0	445 $\pm$ 14	—	0.20 $\pm$ 0.0	0.91 $\pm$ 0.0	2269 $\pm$ 52	—
AVICI		0.01 $\pm$ 0.0	0.68 $\pm$ 0.0	411 $\pm$ 7	0.62 $\pm$ 0.0	0.01 $\pm$ 0.0	0.46 $\pm$ 0.0	1614 $\pm$ 21	0.47 $\pm$ 0.0
SEA (FCI)		0.49 $\pm$ 0.2	0.93 $\pm$ 0.1	314 $\pm$ 107	0.61 $\pm$ 0.1	0.56 $\pm$ 0.1	0.90 $\pm$ 0.1	1103 $\pm$ 190	0.75 $\pm$ 0.1
SEA (GIES)		<b>0.70</b> $\pm$ 0.1	<b>0.99</b> $\pm$ 0.0	<b>226</b> $\pm$ 57	<b>0.71</b> $\pm$ 0.1	<b>0.70</b> $\pm$ 0.0	<b>0.94</b> $\pm$ 0.0	<b>872</b> $\pm$ 44	<b>0.80</b> $\pm$ 0.0
500		INVCOV	0.47 $\pm$ 0.0	1.00 $\pm$ 0.0	504 $\pm$ 19	—	0.38 $\pm$ 0.0	0.99 $\pm$ 0.0	2300 $\pm$ 34
	CORR	0.42 $\pm$ 0.0	1.00 $\pm$ 0.0	543 $\pm$ 18	—	0.21 $\pm$ 0.0	0.93 $\pm$ 0.0	2790 $\pm$ 78	—
	AVICI	0.00 $\pm$ 0.0	0.70 $\pm$ 0.0	497 $\pm$ 19	<b>0.63</b> $\pm$ 0.0	0.01 $\pm$ 0.0	0.48 $\pm$ 0.0	2004 $\pm$ 25	0.48 $\pm$ 0.0
	SEA (FCI)	0.27 $\pm$ 0.1	0.90 $\pm$ 0.1	758 $\pm$ 297	0.51 $\pm$ 0.0	0.29 $\pm$ 0.1	0.86 $\pm$ 0.1	1824 $\pm$ 273	0.56 $\pm$ 0.1
	SEA (GIES)	<b>0.41</b> $\pm$ 0.2	<b>0.98</b> $\pm$ 0.0	<b>485</b> $\pm$ 170	0.57 $\pm$ 0.1	<b>0.48</b> $\pm$ 0.1	<b>0.92</b> $\pm$ 0.0	<b>1654</b> $\pm$ 505	<b>0.67</b> $\pm$ 0.0

Table 12 shows that despite omitting the DAG constraint, we find that our predicted graphs (test split) are nearly all acyclic, with a naive discretization threshold of 0.5. Unlike Lippe et al. (2022), which also omits the acyclicity constraint during training but optionally enforces it at inference time, we do not require any post-processing to achieve high performance. Empirically, we found existing DAG constraints to be unstable (Lagrangian) and slow to optimize (Zheng et al., 2018; Brouillard et al., 2020). DAG behavior would not emerge until late in training, when the regularization term is of 1e-8 scale or smaller.

Alternatively, we could quantify the raw information content provided by these two features through the INVCOV, FCI\*, and GIES\* baselines (Tables 13, 14, 15, 16). Overall, INVCOV and FCI\* are comparable to worse-performing baselines. GIES\* performs very well, sometimes approaching the strongest baselines. However, there remains a large gap in performance between these ablations and our method, highlighting the value of learning non-linear transformations of these inputs.

Table 10 and Figure 9 show that the current implementations of SEA can generalize to graphs up to  $4\times$  larger than those seen during training. During training, we did not initially anticipate testing on much larger graphs. As a result, there are two minor issues with the current implementation with respect to scaling. First, we set an insufficient maximum subset positional embedding size of 500,

Table 11: Causal discovery ablations by setting hidden representations to zero. Each setting encompasses 5 distinct Erdős-Rényi graphs. The symbol † indicates that SEA was not pretrained on this setting. We set  $T = 100$ .

$N$	$E$	Model	Linear		NN add.		NN non-add.		Sigmoid†		Polynomial†	
			mAP ↑	SHD ↓	mAP ↑	SHD ↓	mAP ↑	SHD ↓	mAP ↑	SHD ↓	mAP ↑	SHD ↓
10	10	SEA (FCI)	0.97	1.6	0.95	2.4	0.92	2.8	0.83	3.7	0.69	6.7
		$h^p \leftarrow 0$	0.20	29.8	0.27	22.4	0.34	24.2	0.26	22.6	0.24	26.0
		$h^E \leftarrow 0$	0.61	24.0	0.71	28.8	0.76	27.8	0.49	26.7	0.51	26.7
		SEA (GIES)	0.99	1.2	0.94	2.6	0.91	3.2	0.85	4.0	0.70	5.8
		$h^p \leftarrow 0$	0.30	29.2	0.27	29.4	0.19	29.0	0.35	27.4	0.31	27.1
		$h^E \leftarrow 0$	0.85	6.4	0.82	10.2	0.78	13.2	0.63	10.2	0.55	13.4
20	80	SEA (FCI)	0.86	29.6	0.55	73.6	0.72	51.8	0.77	42.8	0.61	61.8
		$h^p \leftarrow 0$	0.23	128.4	0.27	110.6	0.22	119.6	0.23	110.7	0.23	111.1
		$h^E \leftarrow 0$	0.79	50.4	0.52	99.6	0.71	76.4	0.58	93.6	0.59	87.5
		SEA (GIES)	0.89	26.8	0.58	71.4	0.73	50.6	0.76	45.0	0.65	60.1
		$h^p \leftarrow 0$	0.25	125.2	0.21	123.0	0.24	113.6	0.27	118.0	0.24	129.8
		$h^E \leftarrow 0$	0.86	35.2	0.55	76.8	0.70	53.4	0.69	47.1	0.59	63.5
100	400	SEA (FCI)	0.90	122.0	0.28	361.2	0.60	273.2	0.69	226.9	0.38	327.0
		$h^p \leftarrow 0$	0.05	726.4	0.04	639.4	0.05	637.0	0.05	760.2	0.04	658.3
		$h^E \leftarrow 0$	0.82	167.4	0.04	403.4	0.51	352.4	0.64	263.8	0.33	366.1
		SEA (GIES)	0.91	116.6	0.27	364.4	0.61	266.8	0.69	218.3	0.38	328.0
		$h^p \leftarrow 0$	0.05	780.0	0.04	846.0	0.05	715.4	0.04	744.4	0.04	769.8
		$h^E \leftarrow 0$	0.86	134.8	0.03	403.4	0.52	357.8	0.67	224.1	0.32	359.6

Table 12: Our predicted graphs are highly acyclic, on synthetic ER test sets.

$N$	Acyclic	Total	Proportion
10	434	440	0.99
20	431	440	0.98
100	433	440	0.98

so it was impossible to encode more subsets. Second, we did not sample random starting subset indices to ensure that higher-order embeddings are updated equally. Since we never sampled up to 500 subsets during training, these higher-order embeddings were essentially random. We anticipate that increasing the limit on the number of subsets and ensuring that all embeddings are sufficiently learned will improve the generalization capacity on larger graphs. Nonetheless, our current model already obtains reasonable performance on larger graphs, out of the box.

Finally, we note that AVICI scales very poorly to graphs significantly beyond the scope of their training set. For example,  $N = 100$  is only  $2\times$  their largest training graphs, but the performance already drops dramatically.

Figure 8 depicts the model runtimes. SEA continues to run quickly on much larger graphs, while AVICI runtimes increase significantly with graph size.

DCDI learns a new generative model over each dataset, and its more powerful, deep sigmoidal flow variant seems to perform well in some (but not all) of these harder cases.

### C.5 Results on real datasets

The Sachs flow cytometry dataset (Sachs et al., 2005) measured the expression of phosphoproteins and phospholipids at the single cell level. We use the subset proposed by Wang et al. (2017). The ground truth “consensus graph” consists of 11 nodes and 17 edges over 5,845 samples, of which 1,755 are observational and 4,091 are interventional. The observational data were generated by a “general perturbation” which activated signaling pathways, and the interventional data were generated by perturbations intended to target individual proteins. Despite the popularity of this dataset in

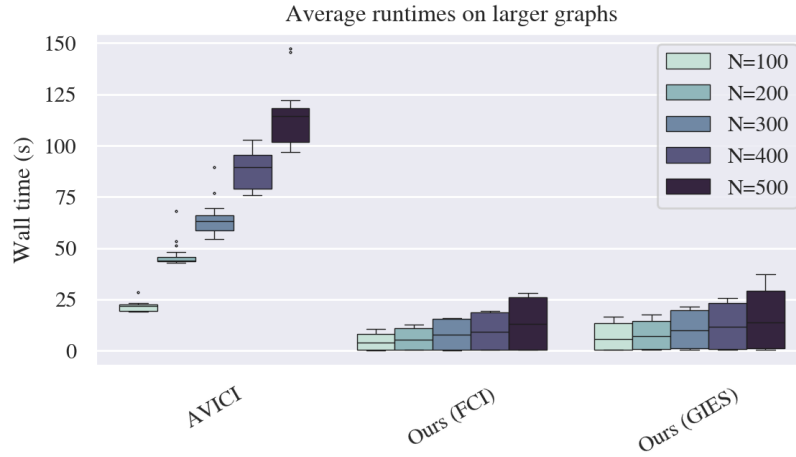


Figure 8: SEA scales very well in terms of runtime on much larger graphs, while AVICI runtimes suffer as graph sizes increase.

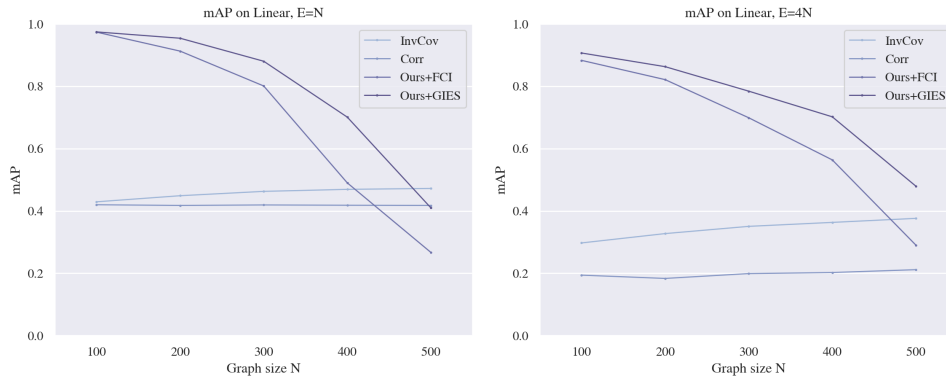


Figure 9: mAP on graphs larger than seen during training. During training, we only sampled a maximum of 100 subsets, so performance drop may be due to extrapolation beyond trained embeddings. We did not have time to finetune these embeddings for more samples. These values correspond to the numbers in Table 10.

causal discovery literature (due to lack of better alternatives), biological networks are known to be time-resolved and cyclic, so the validity of the ground truth “consensus” graph has been questioned by experts Mooij et al. (2020). Nonetheless, we benchmark all methods on this dataset in Table 19.

Table 13: Full results on synthetic datasets (continuous metrics). Each setting encompasses 5 distinct Erdős-Rényi graphs. † indicates that this setting is o.o.d. \* indicates non-parametric bootstrapping. All standard deviations were within 0.03 (most within 0.01).

$N$	$E$	Model	Linear		NN add.		NN non-add.		Sigmoid†		Polynomial†			
			mAP ↑	AUC ↑										
10	10	DCCI-G	0.74	0.88	0.79	0.91	0.89	0.95	0.46	0.72	0.41	0.68		
		DCCI-DSF	0.82	0.92	0.57	0.83	0.50	0.81	0.38	0.69	0.29	0.64		
		DCD-FG	0.45	0.68	0.41	0.67	0.59	0.79	0.40	0.64	0.50	0.72		
		DIFFAN	0.25	0.73	0.32	0.70	0.12	0.51	0.24	0.70	0.20	0.65		
		DECI	0.18	0.63	0.16	0.63	0.23	0.71	0.29	0.72	0.46	0.83		
		AVICI	0.45	0.80	0.81	0.97	0.65	0.89	0.52	0.81	0.31	0.70		
		VARSORT*	0.70	0.84	0.76	0.90	0.83	0.93	0.52	0.72	0.40	0.71		
		INVCov	0.46	0.88	0.43	0.86	0.34	0.81	0.43	0.86	0.43	0.83		
		FCI*	0.52	0.78	0.38	0.71	0.40	0.70	0.56	0.79	0.41	0.71		
		GIES*	0.81	0.96	0.61	0.93	0.71	0.92	0.70	0.95	0.61	0.87		
		SEA (FCI)	0.98	1.00	0.88	0.98	0.88	0.97	0.83	<b>0.97</b>	0.62	0.88		
		SEA (GIES)	<b>0.99</b>	<b>1.00</b>	<b>0.94</b>	<b>0.99</b>	<b>0.91</b>	<b>0.98</b>	<b>0.85</b>	0.97	<b>0.70</b>	<b>0.89</b>		
		10	40	DCCI-G	0.65	0.72	0.65	0.74	0.84	0.88	0.54	0.59	0.56	0.61
				DCCI-DSF	0.65	0.72	0.59	0.67	0.84	0.90	0.52	0.58	0.57	0.62
DCD-FG	0.51			0.57	0.57	0.63	0.53	0.59	0.65	0.68	0.65	0.68		
DIFFAN	0.40			0.49	0.36	0.37	0.41	0.53	0.40	0.45	0.37	0.40		
DECI	0.45			0.49	0.50	0.58	0.44	0.52	0.53	0.61	0.63	0.72		
AVICI	0.46			0.47	0.63	0.65	0.79	0.86	0.49	0.53	0.47	0.55		
VARSORT*	0.81			0.83	0.87	0.89	0.71	0.73	0.69	0.72	0.56	0.62		
INVCov	0.49			0.57	0.46	0.50	0.46	0.53	0.47	0.50	0.48	0.53		
FCI*	0.43			0.50	0.50	0.53	0.46	0.52	0.50	0.51	0.45	0.50		
GIES*	0.49			0.53	0.56	0.64	0.49	0.53	0.44	0.46	0.61	0.62		
SEA (FCI)	0.83			0.85	0.85	0.89	0.86	0.90	0.74	0.75	0.69	0.67		
SEA (GIES)	<b>0.94</b>			<b>0.95</b>	<b>0.91</b>	<b>0.94</b>	<b>0.89</b>	<b>0.92</b>	<b>0.81</b>	<b>0.85</b>	<b>0.89</b>	<b>0.92</b>		
20	20			DCCI-G	0.59	0.87	0.78	0.94	0.75	0.91	0.36	0.81	0.42	0.74
				DCCI-DSF	0.66	0.89	0.69	0.91	0.41	0.83	0.37	0.82	0.26	0.71
		DCD-FG	0.48	0.85	0.58	0.91	0.51	0.87	0.50	0.78	0.44	0.76		
		DIFFAN	0.19	0.73	0.16	0.69	0.20	0.72	0.29	0.79	0.09	0.65		
		DECI	0.14	0.70	0.14	0.72	0.16	0.73	0.24	0.79	0.35	0.84		
		AVICI	0.48	0.87	0.59	0.91	0.67	0.90	0.42	0.84	0.24	0.69		
		VARSORT*	0.81	0.91	0.81	0.92	0.57	0.83	0.50	0.76	0.33	0.69		
		INVCov	0.40	0.90	0.31	0.90	0.31	0.84	0.42	0.92	0.41	0.87		
		FCI*	0.66	0.86	0.42	0.74	0.40	0.77	0.56	0.80	0.41	0.76		
		GIES*	0.84	0.99	0.79	0.97	0.56	0.93	0.71	0.97	0.62	0.91		
		SEA (FCI)	0.96	<b>1.00</b>	0.91	0.99	0.82	<b>0.97</b>	<b>0.85</b>	<b>0.98</b>	<b>0.69</b>	0.91		
		SEA (GIES)	<b>0.97</b>	<b>1.00</b>	<b>0.94</b>	<b>0.99</b>	<b>0.83</b>	0.97	0.84	0.97	0.69	<b>0.92</b>		
		20	80	DCCI-G	0.46	0.73	0.41	0.71	<b>0.82</b>	<b>0.93</b>	0.48	0.71	0.37	0.62
				DCCI-DSF	0.48	0.75	0.44	0.74	0.74	0.92	0.48	0.71	0.38	0.63
DCD-FG	0.32			0.61	0.33	0.64	0.41	0.73	0.47	0.74	0.49	0.69		
DIFFAN	0.21			0.53	0.19	0.41	0.18	0.46	0.22	0.55	0.18	0.37		
DECI	0.25			0.57	0.29	0.61	0.26	0.59	0.31	0.66	0.43	0.73		
AVICI	0.34			0.63	0.46	0.73	0.49	0.74	0.34	0.64	0.30	0.59		
VARSORT*	0.76			0.86	0.50	0.81	0.47	0.69	0.59	0.76	0.38	0.63		
INVCov	0.36			0.72	0.26	0.54	0.30	0.64	0.35	0.72	0.32	0.61		
FCI*	0.30			0.59	0.31	0.57	0.30	0.59	0.41	0.66	0.34	0.61		
GIES*	0.41			0.75	0.44	0.74	0.46	0.73	0.50	0.78	0.49	0.69		
SEA (FCI)	0.80			0.92	0.55	0.81	0.70	0.89	0.74	0.85	0.55	0.67		
SEA (GIES)	<b>0.89</b>			<b>0.95</b>	<b>0.58</b>	<b>0.84</b>	0.73	0.90	<b>0.76</b>	<b>0.90</b>	<b>0.65</b>	<b>0.84</b>		

Table 14: Full results on synthetic datasets (discrete metrics). Each setting encompasses 5 distinct Erdős-Rényi graphs. † indicates that this setting is o.o.d. \* indicates non-parametric bootstrapping. All OA standard deviations were within 0.2.

$N$	$E$	Model	Linear		NN add.		NN non-add.		Sigmoid†		Polynomial†			
			OA ↑	SHD ↓	OA ↑	SHD ↓	OA ↑	SHD ↓	OA ↑	SHD ↓	OA ↑	SHD ↓		
10	10	DCDI-G	0.73	2.8±2	0.84	<b>2.2</b> ±3	0.88	<b>1.0</b> ±1	0.46	5.8±3	0.33	8.9±6		
		DCDI-DSF	0.81	2.0±3	0.73	3.0±3	0.60	4.2±1	0.43	6.3±3	0.24	11.2±5		
		DCD-FG	0.50	20.4±3	0.47	21.2±4	0.70	19.2±4	0.43	19.8±4	0.54	18.5±5		
		DIFFAN	0.61	14.0±5	0.55	13.6±14	0.26	21.8±8	0.53	12.0±5	0.47	15.0±6		
		DECI	0.50	19.4±5	0.43	13.8±6	0.62	16.2±3	0.63	13.9±7	0.75	7.8±4		
		AVICI	0.58	8.2±4	0.79	4.2±3	0.65	5.6±3	0.54	8.3±3	0.35	9.6±4		
		VARSORT*	0.70	6.0±2	0.74	4.0±2	0.90	4.2±3	0.52	7.6±3	0.48	9.3±3		
		INVCOV	—	10.6±3	—	10.2±6	—	13.6±3	—	11.1±4	—	10.4±3		
		FCI*	0.52	10.0±3	0.43	8.2±4	0.41	9.8±2	0.55	9.1±3	0.40	10.0±4		
		GIES*	0.76	3.6±2	0.49	6.0±5	0.69	4.8±2	0.67	5.9±3	0.63	7.1±3		
		SEA (FCI)	0.93	<b>1.0</b> ±1	0.82	3.0±4	0.90	3.8±2	0.73	<b>3.9</b> ±2	0.70	6.1±3		
		SEA (GIES)	<b>0.94</b>	1.2±1	<b>0.88</b>	2.6±4	<b>0.93</b>	3.2±1	<b>0.84</b>	4.0±3	<b>0.79</b>	<b>5.8</b> ±3		
		10	40	DCDI-G	0.50	19.8±2	0.64	17.4±3	0.82	8.0±2	0.25	30.8±4	0.23	31.0±2
				DCDI-DSF	0.48	19.8±3	0.55	21.6±7	0.87	<b>6.0</b> ±3	0.25	31.4±3	0.25	30.0±3
DCD-FG	0.35			28.6±4	0.40	26.0±1	0.36	26.8±4	0.45	24.4±5	0.41	25.5±4		
DIFFAN	0.41			27.6±4	0.29	33.4±4	0.49	26.4±4	0.38	29.4±6	0.32	31.8±4		
DECI	0.43			27.6±5	0.55	22.4±4	0.50	25.4±3	0.54	<b>21.5</b> ±3	0.57	<b>18.4</b> ±3		
AVICI	0.44			33.0±5	0.68	28.4±7	0.85	20.0±4	0.50	35.0±3	0.50	38.8±2		
VARSORT*	0.76			21.8±5	0.81	15.4±4	0.61	24.0±4	0.67	33.6±5	0.46	37.6±2		
INVCOV	—			40.2±2	—	44.6±2	—	41.0±3	—	44.2±3	—	42.3±2		
FCI*	0.16			39.2±2	0.24	38.8±3	0.22	36.2±3	0.22	38.8±2	0.16	39.9±2		
GIES*	0.44			33.4±4	0.60	33.0±5	0.51	32.0±3	0.38	36.7±2	0.63	34.6±3		
SEA (FCI)	0.80			18.6±2	0.89	15.4±4	0.87	18.8±4	0.78	24.4±6	0.69	26.9±4		
SEA (GIES)	<b>0.91</b>			<b>12.8</b> ±4	<b>0.95</b>	<b>10.4</b> ±6	<b>0.89</b>	17.2±3	<b>0.87</b>	24.5±3	<b>0.93</b>	29.5±3		
20	20			DCDI-G	0.75	6.4±2	0.90	<b>3.0</b> ±2	0.84	<b>4.4</b> ±2	0.39	42.7±6	0.48	10.4±3
				DCDI-DSF	0.77	5.2±3	0.85	4.2±4	0.64	11.6±3	0.41	43.2±6	0.45	15.7±5
		DCD-FG	0.76	51.2±12	0.88	177±57	0.85	193±27	0.65	251±35	0.60	52.7±19		
		DIFFAN	0.56	40.2±27	0.47	38.6±26	0.53	35.0±26	0.63	19.2±8	0.42	49.7±15		
		DECI	0.54	52.0±17	0.56	41.0±14	0.56	39.0±8	0.65	30.0±9	0.73	18.9±6		
		AVICI	0.56	17.2±5	0.69	10.8±2	0.79	11.2±3	0.53	17.2±5	0.37	18.4±4		
		VARSORT*	0.84	10.0±3	0.88	6.6±6	0.74	14.6±8	0.50	16.1±4	0.40	17.1±4		
		INVCOV	—	23.6±6	—	24.6±5	—	24.6±6	—	22.9±5	—	20.0±5		
		FCI*	0.70	19.0±5	0.45	17.4±2	0.50	19.4±6	0.57	18.5±4	0.44	18.9±5		
		GIES*	0.80	7.4±2	0.77	9.0±5	0.71	14.0±3	0.75	12.5±4	0.68	13.7±4		
		SEA (FCI)	<b>0.92</b>	3.2±3	0.93	5.0±3	0.94	8.8±3	0.79	<b>6.7</b> ±3	0.76	<b>9.8</b> ±4		
		SEA (GIES)	0.89	<b>3.0</b> ±1	<b>0.95</b>	3.4±2	<b>0.94</b>	7.8±3	<b>0.83</b>	8.1±3	<b>0.78</b>	10.1±4		
		20	80	DCDI-G	0.54	44.0±6	0.53	61.6±11	0.89	37.4±34	0.46	44.2±5	0.26	59.7±5
				DCDI-DSF	0.57	41.2±3	0.61	<b>60.0</b> ±12	0.85	<b>28.4</b> ±26	0.47	43.6±6	0.30	57.6±5
DCD-FG	0.58			172±27	0.65	156±41	0.75	162±49	0.62	80.1±13	0.48	79.8±7		
DIFFAN	0.46			127±5	0.28	154±10	0.36	145±7	0.45	117±21	0.21	157±7		
DECI	0.30			87.2±3	0.47	104±7	0.35	79.6±9	0.48	71.0±7	0.57	58.9±11		
AVICI	0.51			75.6±10	0.69	72.8±6	0.69	61.2±10	0.50	70.6±6	0.50	75.5±7		
VARSORT*	0.82			44.8±4	0.84	73.6±13	0.61	65.2±10	0.67	63.4±5	0.39	75.6±5		
INVCOV	—			97.6±6	—	121±4	—	104±9	—	95.6±7	—	97.8±4		
FCI*	0.19			75.8±11	0.19	80.2±5	0.22	74.4±8	0.33	72.3±6	0.23	76.6±5		
GIES*	0.56			70.0±11	0.73	75.2±4	0.59	67.4±7	0.62	65.6±7	0.61	68.1±5		
SEA (FCI)	0.86			39.8±12	0.87	73.8±12	<b>0.92</b>	52.0±9	0.82	<b>42.9</b> ±6	0.69	<b>57.0</b> ±5		
SEA (GIES)	<b>0.92</b>			<b>26.8</b> ±8	<b>0.88</b>	71.4±8	<b>0.92</b>	50.6±7	<b>0.84</b>	45.0±7	<b>0.89</b>	60.1±6		

Table 15: Full results on synthetic datasets (continuous metrics). Each setting encompasses 5 distinct scale-free graphs. † indicates that this setting is o.o.d. \* indicates non-parametric bootstrapping. All standard deviations were within 0.02.

$N$	$E$	Model	Linear		NN add.		NN non-add.		Sigmoid†		Polynomial†			
			mAP ↑	AUC ↑										
10	10	DCCI-G	0.54	0.90	0.59	0.88	0.69	0.89	0.48	0.77	0.50	0.73		
		DCCI-DSF	0.70	0.92	0.71	0.88	0.36	0.83	0.46	0.75	0.49	0.76		
		DCD-FG	0.56	0.76	0.47	0.72	0.50	0.73	0.44	0.68	0.57	0.75		
		DIFFAN	0.25	0.73	0.15	0.66	0.16	0.62	0.31	0.75	0.24	0.63		
		DECI	0.17	0.65	0.17	0.67	0.20	0.72	0.27	0.73	0.49	0.82		
		AVICI	0.51	0.87	0.55	0.85	0.76	0.95	0.44	0.81	0.27	0.71		
		VARSORT*	0.67	0.84	0.69	0.86	0.76	0.88	0.45	0.69	0.46	0.73		
		INVCOV	0.50	0.92	0.41	0.87	0.38	0.84	0.47	0.90	0.45	0.86		
		FCI*	0.56	0.80	0.51	0.80	0.43	0.74	0.60	0.82	0.34	0.68		
		GIES*	0.87	0.98	0.61	0.94	0.69	0.94	0.75	0.96	0.71	<b>0.91</b>		
		SEA (FCI)	<b>0.96</b>	<b>0.99</b>	0.88	0.98	0.88	0.97	0.79	0.96	0.73	0.90		
		SEA (GIES)	0.95	<b>0.99</b>	<b>0.94</b>	<b>0.98</b>	<b>0.92</b>	<b>0.98</b>	<b>0.85</b>	<b>0.98</b>	<b>0.74</b>	0.90		
		10	40	DCCI-G	0.70	0.85	0.74	0.85	<b>0.88</b>	<b>0.91</b>	0.56	0.66	0.53	0.64
				DCCI-DSF	0.74	0.87	0.73	0.84	0.71	0.90	0.56	0.69	0.51	0.63
DCD-FG	0.37			0.58	0.45	0.61	0.45	0.58	0.49	0.63	0.63	0.73		
DIFFAN	0.29			0.50	0.25	0.38	0.28	0.46	0.31	0.53	0.27	0.44		
DECI	0.30			0.51	0.41	0.65	0.33	0.51	0.38	0.60	0.59	0.77		
AVICI	0.41			0.57	0.65	0.81	0.55	0.67	0.41	0.59	0.40	0.61		
VARSORT*	0.77			0.83	0.74	0.87	0.59	0.71	0.66	0.76	0.50	0.66		
INVCOV	0.44			0.71	0.38	0.59	0.42	0.62	0.44	0.67	0.42	0.62		
FCI*	0.47			0.64	0.41	0.60	0.40	0.58	0.48	0.64	0.41	0.59		
GIES*	0.43			0.68	0.43	0.63	0.44	0.61	0.49	0.69	0.59	0.71		
SEA (FCI)	0.85			0.91	0.80	0.90	0.77	0.88	0.76	0.83	0.66	0.71		
SEA (GIES)	<b>0.92</b>			<b>0.96</b>	<b>0.84</b>	<b>0.93</b>	0.83	0.90	<b>0.79</b>	<b>0.88</b>	<b>0.78</b>	<b>0.87</b>		
20	20			DCCI-G	0.41	0.95	0.50	0.94	0.69	0.96	0.37	0.83	0.37	0.77
				DCCI-DSF	0.48	0.95	0.55	0.93	0.33	0.90	0.37	0.79	0.35	0.82
		DCD-FG	0.51	0.87	0.39	0.83	0.48	0.84	0.56	0.84	0.50	0.84		
		DIFFAN	0.27	0.80	0.11	0.65	0.11	0.66	0.26	0.77	0.12	0.69		
		DECI	0.13	0.69	0.15	0.71	0.15	0.73	0.15	0.71	0.25	0.79		
		AVICI	0.53	0.88	0.66	0.89	0.74	0.92	0.46	0.87	0.32	0.77		
		VARSORT*	0.67	0.85	0.84	0.93	0.59	0.86	0.45	0.72	0.44	0.73		
		INVCOV	0.44	0.94	0.35	0.91	0.30	0.89	0.43	0.93	0.41	0.87		
		FCI*	0.63	0.84	0.44	0.78	0.43	0.79	0.60	0.86	0.47	0.78		
		GIES*	0.82	0.99	0.58	0.95	0.57	0.96	0.75	0.98	0.61	0.90		
		SEA (FCI)	<b>0.94</b>	<b>1.00</b>	0.87	<b>0.98</b>	0.83	0.97	<b>0.82</b>	<b>0.98</b>	<b>0.72</b>	<b>0.92</b>		
		SEA (GIES)	0.93	<b>1.00</b>	<b>0.91</b>	0.98	<b>0.88</b>	<b>0.98</b>	<b>0.82</b>	0.98	0.70	0.91		
		20	80	DCCI-G	0.62	0.88	0.61	<b>0.89</b>	<b>0.76</b>	<b>0.94</b>	0.44	0.76	0.36	0.60
				DCCI-DSF	0.58	0.87	0.55	0.86	0.58	0.92	0.43	0.78	0.35	0.66
DCD-FG	0.38			0.70	0.30	0.69	0.48	0.80	0.48	0.75	0.53	0.73		
DIFFAN	0.18			0.55	0.15	0.44	0.16	0.53	0.19	0.56	0.15	0.38		
DECI	0.21			0.58	0.24	0.64	0.26	0.66	0.30	0.68	0.41	0.75		
AVICI	0.29			0.61	0.54	0.80	0.60	0.85	0.35	0.65	0.28	0.63		
VARSORT*	0.79			0.90	0.57	0.83	0.62	0.81	0.57	0.77	0.38	0.64		
INVCOV	0.38			0.81	0.22	0.56	0.32	0.73	0.38	0.78	0.33	0.67		
FCI*	0.31			0.63	0.30	0.62	0.30	0.62	0.41	0.68	0.32	0.62		
GIES*	0.51			0.87	0.43	0.78	0.47	0.81	0.52	0.82	0.47	0.73		
SEA (FCI)	0.87			0.96	0.59	0.87	0.70	0.90	0.73	0.87	0.53	0.71		
SEA (GIES)	<b>0.92</b>			<b>0.98</b>	<b>0.63</b>	0.89	0.73	0.91	<b>0.77</b>	<b>0.92</b>	<b>0.62</b>	<b>0.84</b>		

Table 16: Full results on synthetic datasets (discrete metrics). Each setting encompasses 5 distinct scale-free graphs. † indicates that this setting is o.o.d. \* indicates non-parametric bootstrapping. All OA standard deviations were within 0.2.

$N$	$E$	Model	Linear		NN add.		NN non-add.		Sigmoid†		Polynomial†			
			OA ↑	SHD ↓										
10	10	DCCI-G	0.51	16.6±1	0.61	17.4±2	0.71	16.2±2	0.59	16.9±5	0.63	16.6±3		
		DCCI-DSF	0.70	16.2±2	0.75	15.4±3	0.36	16.8±2	0.48	18.1±3	0.67	18.0±2		
		DCD-FG	0.60	16.4±5	0.57	22.2±4	0.57	20.0±4	0.47	17.9±4	0.59	16.8±5		
		DIFFAN	0.55	9.2±4	0.49	14.6±4	0.36	11.6±4	0.59	7.7±4	0.42	14.8±6		
		DECI	0.51	17.4±5	0.55	17.4±5	0.58	12.0±2	0.62	12.6±5	0.74	8.2±6		
		AVICI	0.64	6.8±3	0.59	5.4±3	0.77	3.6±1	0.48	7.8±3	0.35	9.5±3		
		VARSORT*	0.82	4.4±1	0.78	4.8±2	0.80	3.4±2	0.47	7.3±3	0.55	8.1±3		
		INVCOV	—	8.8±3	—	9.2±2	—	9.8±1	—	9.7±3	—	10.2±2		
		FCI*	0.62	8.4±2	0.51	7.8±2	0.45	8.0±2	0.61	9.2±3	0.34	9.6±2		
		GIES*	0.83	2.2±2	0.60	6.0±2	0.75	4.2±2	0.72	4.9±3	0.73	5.7±2		
		SEA (FCI)	<b>0.89</b>	<b>1.4±2</b>	0.90	2.6±2	0.93	2.2±1	0.71	4.0±3	0.72	5.2±2		
		SEA (GIES)	0.85	<b>1.4±1</b>	<b>0.96</b>	<b>1.8±1</b>	<b>0.94</b>	<b>2.0±1</b>	<b>0.86</b>	<b>3.4±3</b>	<b>0.83</b>	<b>5.0±2</b>		
		10	40	DCCI-G	0.82	24.0±4	0.85	27.8±5	0.87	19.6±2	0.62	31.4±3	0.52	32.6±4
				DCCI-DSF	0.79	22.8±5	0.79	24.4±4	0.82	20.4±2	0.64	31.6±2	0.58	33.3±3
DCD-FG	0.36			24.8±4	0.41	25.2±5	0.38	25.6±8	0.41	23.2±6	0.54	18.5±3		
DIFFAN	0.40			29.8±8	0.28	37.0±2	0.38	32.6±2	0.45	28.0±6	0.33	32.7±5		
DECI	0.43			27.8±3	0.66	22.6±3	0.48	28.6±3	0.52	22.2±4	0.66	<b>13.3±3</b>		
AVICI	0.43			20.2±4	0.84	17.2±4	0.61	20.4±8	0.52	24.8±3	0.49	26.5±2		
VARSORT*	0.75			13.4±2	0.89	<b>12.6±2</b>	0.60	20.6±3	0.65	20.8±4	0.50	26.4±2		
INVCOV	—			31.4±3	—	37.2±4	—	36.0±4	—	32.3±5	—	34.8±3		
FCI*	0.33			23.8±2	0.28	27.2±2	0.25	27.6±4	0.36	26.1±2	0.24	27.3±2		
GIES*	0.46			21.8±3	0.50	24.4±2	0.48	25.2±5	0.52	22.7±3	0.64	22.5±2		
SEA (FCI)	0.80			10.0±4	0.88	14.0±2	0.87	15.8±3	0.79	15.6±3	0.64	18.5±3		
SEA (GIES)	<b>0.88</b>			<b>6.6±3</b>	<b>0.98</b>	14.0±5	<b>0.88</b>	<b>14.4±3</b>	<b>0.87</b>	<b>14.1±3</b>	<b>0.93</b>	19.1±3		
20	20			DCCI-G	0.54	40.4±2	0.70	44.8±8	0.88	39.8±6	0.47	41.1±4	0.53	38.4±6
				DCCI-DSF	0.64	40.4±3	0.65	42.4±8	0.40	42.2±8	0.37	41.1±4	0.45	49.3±18
		DCD-FG	0.68	252±23	0.77	183±52	0.78	181±27	0.70	251±45	0.69	278±68		
		DIFFAN	0.67	23.6±13	0.40	42.2±22	0.42	34.0±11	0.59	22.6±12	0.50	46.8±13		
		DECI	0.50	42.0±5	0.54	43.0±11	0.57	40.0±13	0.51	34.7±7	0.65	25.3±6		
		AVICI	0.68	11.8±3	0.79	9.2±2	0.80	7.8±2	0.60	15.3±4	0.45	18.3±5		
		VARSORT*	0.74	10.4±3	0.91	6.2±2	0.76	13.0±6	0.49	13.7±4	0.51	16.7±6		
		INVCOV	—	20.2±3	—	24.4±5	—	23.8±5	—	21.2±4	—	20.8±5		
		FCI*	0.67	13.8±2	0.52	17.4±1	0.53	17.8±5	0.65	16.7±4	0.50	18.9±5		
		GIES*	0.82	6.4±3	0.71	12.6±2	0.68	13.2±3	0.75	11.4±5	0.73	13.4±4		
		SEA (FCI)	<b>0.90</b>	<b>2.8±1</b>	0.87	7.0±2	0.91	8.2±5	0.73	<b>7.7±3</b>	0.71	<b>9.5±4</b>		
		SEA (GIES)	0.85	4.0±2	<b>0.95</b>	<b>3.6±2</b>	<b>0.93</b>	<b>6.2±4</b>	<b>0.80</b>	7.9±4	<b>0.82</b>	9.9±3		
		20	80	DCCI-G	0.81	93.0±10	0.73	104±7	<b>0.91</b>	67.8±8	0.61	82.5±8	0.53	79.7±5
				DCCI-DSF	0.75	103±7	0.73	94.8±11	0.77	63.8±7	0.65	84.4±8	0.52	82.6±5
DCD-FG	0.63			188±24	0.70	187±14	0.78	190±26	0.71	217±38	0.71	235±32		
DIFFAN	0.42			111±18	0.30	145±11	0.40	119±13	0.41	100±22	0.21	149±11		
DECI	0.33			72.2±10	0.48	81.4±10	0.48	67.0±9	0.50	60.4±12	0.58	<b>47.2±7</b>		
AVICI	0.45			56.0±5	0.77	<b>47.6±8</b>	0.76	42.6±3	0.50	54.0±6	0.47	62.2±5		
VARSORT*	0.85			32.4±5	0.84	54.8±8	0.75	40.2±6	0.64	54.0±6	0.37	60.1±5		
INVCOV	—			79.4±6	—	106±5	—	87.4±2	—	78.8±9	—	86.2±4		
FCI*	0.26			58.2±6	0.22	58.4±4	0.26	55.0±7	0.37	59.3±6	0.23	62.9±4		
GIES*	0.65			48.4±5	0.71	53.6±3	0.68	48.0±4	0.64	53.6±6	0.61	54.9±5		
SEA (FCI)	0.91			25.6±6	0.88	51.6±6	0.89	42.2±4	0.83	36.1±6	0.71	47.4±5		
SEA (GIES)	<b>0.92</b>			<b>17.6±3</b>	<b>0.93</b>	49.2±9	0.89	<b>37.2±5</b>	<b>0.88</b>	<b>35.1±7</b>	<b>0.89</b>	48.1±5		

Table 17: Causal discovery results on synthetic datasets with 100 nodes, continuous metrics. Each setting encompasses 5 distinct Erdős-Rényi graphs. The symbol † indicates that the model was not trained on this setting. All standard deviations were within 0.1.

$N$	$E$	Model	Linear		NN add.		NN non-add.		Sigmoid†		Polynomial†	
			mAP ↑	AUC ↑	mAP ↑	AUC ↑	mAP ↑	AUC ↑	mAP ↑	AUC ↑	mAP ↑	AUC ↑
100	100	DCD-FG	0.11	0.75	0.12	0.71	0.18	0.73	0.20	0.72	0.06	0.60
		INVCov	0.40	0.99	0.22	0.94	0.16	0.87	0.40	0.97	0.36	0.90
		SEA (FCI)	0.96	1.00	0.83	0.97	0.75	0.97	0.79	0.97	0.56	0.88
		SEA (GIES)	0.97	1.00	0.82	0.98	0.74	0.96	0.80	0.97	0.54	0.85
100	400	DCD-FG	0.05	0.59	0.07	0.64	0.10	0.72	0.13	0.72	0.12	0.64
		INVCov	0.25	0.91	0.09	0.62	0.14	0.77	0.27	0.86	0.20	0.67
		SEA (FCI)	0.90	0.99	0.28	0.82	0.60	0.92	0.69	0.92	0.38	0.80
		SEA (GIES)	0.91	0.99	0.27	0.82	0.61	0.92	0.69	0.91	0.38	0.78

Table 18: Causal discovery results on synthetic datasets with 100 nodes, discrete metrics. Each setting encompasses 5 distinct Erdős-Rényi graphs. The symbol † indicates that the model was not trained on this setting.

$N$	$E$	Model	Linear		NN add.		NN non-add.		Sigmoid†		Polynomial†	
			OA ↑	SHD ↓	OA ↑	SHD ↓	OA ↑	SHD ↓	OA ↑	SHD ↓	OA ↑	SHD ↓
100	100	DCD-FG	0.63	3075.8	0.58	2965.0	0.60	2544.4	0.59	3808.0	0.34	1927.9
		INVCov	—	124.4	—	130.0	—	158.8	—	112.3	—	106.3
		SEA (FCI)	0.91	13.4	0.90	34.4	0.91	47.2	0.78	40.3	0.69	59.2
		SEA (GIES)	0.91	13.6	0.93	32.8	0.91	45.8	0.78	38.6	0.68	60.3
100	400	DCD-FG	0.46	3068.2	0.60	3428.8	0.70	3510.8	0.67	3601.8	0.53	3316.7
		INVCov	—	557.0	—	667.8	—	639.0	—	514.7	—	539.4
		SEA (FCI)	0.93	122.0	0.90	361.2	0.91	273.2	0.87	226.9	0.82	327.0
		SEA (GIES)	0.94	116.6	0.91	364.4	0.92	266.8	0.87	218.3	0.84	328.0

Table 19: Complete results on Sachs flow cytometry dataset (Sachs et al., 2005), using the subset proposed by (Wang et al., 2017).

Model	mAP ↑	AUC ↑	SHD ↓
DCDI-G	0.17	0.55	21
DCDI-DSF	0.20	0.59	20
DCD-FG	0.32	0.59	27
DIFFAN	0.14	0.45	37
DECI	0.21	0.62	28
AVICI-L	0.35	0.78	20
AVICI-R	0.29	0.65	18
AVICI-L+R	<b>0.59</b>	<b>0.83</b>	14
FCI*	0.27	0.59	18
GIES*	0.21	0.59	17
SEA (FCI)	0.23	0.54	24
+KCI	0.33	0.63	14
+CORR	0.41	0.70	15
+KCI+CORR	0.49	0.71	<b>13</b>
SEA (GIES)	0.23	0.60	14